TITLE

Stimulating microtubule growth is not the essential function of the microtubule polymerase Stu2

CONDENSED TITLE

Essential regulation of Stu2 nuclear localization

AUTHORS

Joseph S. Carrier[1], Julia R. Torvi[2], Erin Jenson[1], Chloe Jones[1], Binnu Gangadharan[3], Elisabeth A. Geyer[3], Luke M. Rice[3], Brent Lagesse[4] Georjana Barnes[2], Matthew P. Miller[1]*

[1]Department of Biochemistry, University of Utah School of Medicine, Salt Lake City, UT 84112, USA.
[2]Department of Molecular and Cell Biology, University of California, Berkeley, Berkeley, CA 94720, USA.
[3]Departments of Biophysics and Biochemistry, UT Southwestern Medical Center, Dallas, TX 75390, USA.
[4]Division of Computing and Software Systems, School of STEM, University of Washington Bothell, Bothell, WA 98011, USA.

*Correspondence: matthew.miller@biochem.utah.edu (M.P.M.)

SUMMARY

Stu2 is a TOG family protein that performs numerous microtubule regulatory functions in the cell. Here we show that Stu2's nuclear localization is essential for cell viability. Surprisingly, its required nuclear function is distinct from its canonical activities regulating microtubules.

ABSTRACT

TOG family proteins, including the budding yeast Stu2, are essential for the formation of a functional mitotic spindle. Across all eukaryotes, the described functions of this family depend on two microtubule binding elements: TOG domain arrays, and a basic linker domain important for binding the microtubule lattice. Consistently, we find here that Stu2's basic linker is required for its ability to regulate microtubules in vitro, including stimulating microtubule growth, shrinkage, and catastrophe. We furthermore define a region contained within Stu2's basic linker domain as its nuclear localization sequence, and identify phospho-regulation that promotes mitosis-specific nuclear import. Surprisingly, directing nuclear localization is the only function contained within Stu2's basic linker that is required for cell viability, indicating that microtubule lattice binding is not required for Stu2's essential function. Considering that lattice binding is required to stimulate microtubule polymerization and depolymerization in vitro, these established activities are unlikely to be the essential functions carried out by Stu2 in the cell's nucleus.

INTRODUCTION

Cells use a microtubule cytoskeleton that provides shape and structure to the cell, and facilitates the transport of organelles. This dynamic microtubule cytoskeleton is altered to accomplish various functions at different cell cycle stages. During interphase in yeast, a few microtubules extend from the unipolar microtubule organizing center, and are required for nuclear fusion (karyogamy) and ultimately important for nuclear positioning (Tran et al., 2001; van der Vaart et al., 2017). As the cell progresses into mitosis the cell must generate a mitotic spindle to accurately segregate chromosome pairs into the two newly forming cells. This process involves diverse microtubule functions including forming and orienting a bipolar mitotic spindle, establishing correct interactions between kinetochores and microtubules, and elongating the mitotic spindle to separate replicated chromosomes during anaphase (Hagan & Hyams, 1988; Hayles et al., 1994; Kirschner & Mitchison, 1986).

The proper formation of the mitotic spindle requires the function of microtubule associated proteins (MAPs), which regulate the structure and function of the cytoskeleton as the cell progresses through mitosis. MAPs can perform diverse roles in regulating microtubules including nucleation, polymerization and depolymerization, and altering microtubule dynamics (e.g. the frequency of switching between microtubule assembly and disassembly, known as catastrophes and rescues; reviewed in Gudimchuk & McIntosh, 2021). They also act as linkers between microtubules and other cellular elements, and regulate other MAPs often by directing cellular localization (Bodakuntla et al., 2019).

One such family of MAPs is the TOG family of proteins, which conduct conserved functions across all eukaryotes (Al-Bassam & Chang, 2011; Kinoshita et al., 2002; Ohkura et al., 2001). This family of proteins is canonically known for their microtubule polymerase function; however, TOG proteins have additional roles in the cell, including nucleating and anchoring microtubules, regulating kinetochore-microtubule interactions, and regulating the dynamics and disassembly of microtubules (Chen et al., 1998; Geyer et al., 2018; Humphrey et al., 2018; King et al., 2020, 2021; Kinoshita et al., 2002; Kosco et al., 2001; Miller et al., 2016; Podolski et al., 2014; Severin et al., 2001; Wang & Huffaker, 1997). They use conserved TOG domains to bind tubulin heterodimers at or near microtubule plus ends, where they stimulate large changes in the addition or loss of tubulin subunits to the microtubule polymer (Al-Bassam et al., 2006; Ayaz et al., 2014; Brouhard et al., 2008; Geyer et al., 2018; Nithianantham et al., 2018; Podolski et al., 2014; van Breugel et al., 2003; Widlund et al., 2011). In addition to the TOG domains, this family of proteins interacts with the microtubule via a highly basic, linker region. This ‘basic linker’ is critical for their functions, and in fact, is required for most, if not all, of their described activities. First, the basic linker is required for TOG family members to stimulate microtubule assembly in vitro; this domain binds to the microtubule lattice via interactions between positively charged residues in the basic region and the negatively charged E-hooks on the microtubule surface, seemingly to facilitate lattice diffusion and end targeting during microtubule polymerization (Al-Bassam et al., 2006; Geyer et al., 2018; Wang & Huffaker, 1997; Widlund et al., 2011). Second, the basic linker is required for the budding yeast TOG protein, Stu2, together with the γ-tubulin receptor Spc72, to oligomerize the γ-

TuSC for cytoplasmic microtubule nucleation (Gunzelmann et al., 2018). Finally, the kinetochore function of chTOG, the human TOG family member, depends on the presence of either specific residues within, or the entire basic linker domain (Herman et al., 2020). Given these observations across numerous TOG family members, it is not surprising that in budding yeast Stu2, which is to our knowledge the only family member where this has been examined, the basic linker domain is essential for cell viability (Geyer et al., 2018; Gunzelmann et al., 2018; Herman et al., 2020; Miller et al., 2019; Wang & Huffaker, 1997; Widlund et al., 2011). It remains unclear, however, how the basic linker region mechanistically supports each of the TOG protein family's functions, especially given our previous work that suggested specific element(s) within the basic linker region, and not number of positive residues per se, were the important factors determining function (Herman et al., 2020). This apparent discrepancy led us to further examine the role that the basic linker, of the budding yeast Stu2, plays in promoting its cellular function.

Here we identify a conserved patch of amino acids within the basic linker domain of Stu2, that acts as its nuclear localization sequence (NLS). We further discover that phospho-regulation of this NLS, likely by CDK, promotes mitosis-specific nuclear localization. Consistent with our expectations, we find that Stu2's basic linker is required for its ability to regulate microtubules in vitro, including stimulating microtubule assembly, disassembly, and catastrophe. Surprisingly, we find that despite the full basic linker domain being implicated in most, if not all, of Stu2's known microtubule regulatory functions, directing nuclear localization is the only required activity of this domain for cell viability. Thus, Stu2 performs a nuclear function that is essential for cell viability; however, microtubule polymerization and depolymerization, where Stu2 binds to the lattice and adds or subtracts tubulin subunits to the end of a microtubule, is not the required function. Our observations have important implications for understanding what essential function(s) TOG family members carry out in the cell's nucleus.

RESULTS

Two positive residues within a conserved patch of amino acids in Stu2's basic linker region are essential for cell viability.

Stu2 is an essential, multidomain microtubule-associated protein that regulates the microtubule cytoskeleton and is specifically important for generating a functional mitotic spindle (Al-Bassam et al., 2006, p. 2006; Kosco et al., 2001; Pearson et al., 2003). Stu2 contains two amino-terminal TOG domains, and homodimerizes through its coiled-coil domain, allowing for a total of four TOG domains to carry out Stu2's interactions with tubulin heterodimers and microtubules (Fig. 1A). Additionally, Stu2 has a carboxy-terminal binding segment, which facilitates many of Stu2's binding interactions, including interactions with the yeast kinetochore through the Ndc80 complex (Zahm et al., 2021), with the cytoplasmic face of the yeast spindle pole body through Spc72 (Chen et al., 1998; Usui et al., 2003; Wang & Huffaker, 1997) and with the MAPs, Bim1 and Bik1, to regulate microtubule dynamics (Wolyniak et al., 2006). Lastly, Stu2 contains a basic linker region that lies between its TOG and coiled-coil domains (Fig. 1A), which is implicated in many of Stu2's functions (Geyer et al., 2018; Gunzelmann et al., 2018; Herman et al., 2020; Miller et al., 2019; Wang & Huffaker, 1997). It is hypothesized that the quantity of positive charges within this basic linker is critical for Stu2 function (Geyer et al., 2018; Wang & Huffaker, 1997; Widlund et al., 2011). Consistently, the presence and quantity of positive residues is relatively constant across basic linker domains of TOG family members, despite a relative dearth of overall sequence conservation across this region (Fig. S1A). In contrast, we previously observed that specific element(s) within the basic linker region are required for cell viability (Herman et al., 2020), which disagrees with the idea that the quantity of positive residues is the sole factor determining the basic linker's function. These incongruities led us to examine how Stu2's basic linker region supports each of Stu2's functions mechanistically, and whether this domain's function is regulated to alter Stu2's various activities.

We started by examining the conservation across basic linker domains from various fungal species to identify functionally important regions within the basic linker domain. In agreement with previous observations (Herman et al., 2020), there is a conserved 15 residue "patch" within Stu2's basic linker region (Fig. 1B and S1A). This patch is centered on two highly conserved positive residues, K598 and R599, and contains a consensus CDK phosphorylation site, with the sequence S-P-L-R (Fig. 1A; Albuquerque et al., 2008; Holt et al., 2009; Lanz et al., 2021; MacGilvray et al., 2020; Okada et al., 2014; Swaney et al., 2013). To examine if this patch of 15 conserved amino acids is required for cellular function, we performed a serial dilution spot viability assay. Strains contained an endogenously expressed *STU2* allele tagged with an auxin-inducible degron (i.e. *stu2-AID*), allowing for degradation of this copy of Stu2 in the presence of auxin, and expressed mutant variants of *stu2* from an ectopic locus. This combination of *stu2-AID* at the endogenous locus, and ectopic expression of variant *stu2* alleles, will be referred as the "*stu2-AID* system" from now on. As expected, cells expressing a deletion of the entire basic linker (*stu2*$^{\Delta BL}$) displayed viability defects in the presence of auxin (Fig. S1B). Similar to our previous observations, cells expressing a smaller deletion of the above-mentioned conserved patch (*stu2*$^{\Delta 592\text{-}606}$) were inviable, suggesting this conserved

patch of 15 amino acids in the basic linker is necessary for an essential function of Stu2 (Fig. S1B; (Herman et al., 2020). To determine which specific residues within this patch are important, we mutated each of the 15 amino acids in this conserved patch to alanine, and found that two adjacent positive residues, Stu2^{K598} and Stu2^{R599}, were required. Furthermore, we found that alanine mutations of these residues either independently, or together (henceforth referred to as *stu2$^{KR/AA}$*) caused similar viability defects (Fig. 1C-D, Fig. S1C-F).

stu2$^{KR/AA}$ mutants have defects in elongating their mitotic spindle in vivo despite normal microtubule polymerase activity in vitro.

To understand why *stu2$^{KR/AA}$* mutants are inviable, we first asked if expression of this mutant allele resulted in a short mitotic spindle as previously described for loss of function *stu2* mutants (Kosco et al., 2001). To examine this, we used the *stu2-AID* system described above. Additionally, we arrested cells in mitosis by depleting Cdc20 using a *cdc20-AID* allele, and visualized mitotic spindle length using Spc110-mCherry, a component of the spindle pole body. We observed that *STU2^{WT}* cells displayed a bipolar mitotic spindle with an average length (2.00 ± 0.04 µm). In contrast, cells expressing either a full basic linker deletion (i.e. *stu2$^{\Delta BL}$*; 1.57 ± 0.05 µm), a deletion of the conserved patch within the basic linker (*stu2$^{\Delta 592\text{-}606}$*; 1.49 ± 0.06 µm), and *stu2$^{KR/AA}$* (1.39 ± 0.06 µm; Fig. 2A-B) all displayed a significantly shorter mitotic spindle. Furthermore, a significant portion of cells expressing *stu2$^{\Delta BL}$*, *stu2$^{\Delta 592\text{-}606}$, and stu2$^{KR/AA}$* were unable to separate their spindle poles and displayed a single Spc110 focus (8.8%, 14.0%, and 11.0% of cells, respectively), whereas this rarely occurred in *STU2^{WT}* expressing cells (1% of cells; Fig. S2A). These results suggest that Stu2's basic linker region and specifically Stu2$^{K598\ R599}$ are required to establish a normal length metaphase spindle.

We hypothesized that the inability of these Stu2 mutant expressing cells to form a normal length metaphase spindle was due to a disruption in Stu2's microtubule polymerase activity. This idea might be consistent with previous evidence showing a relationship between Stu2's in vitro polymerase activity and the quantity of positively charged residues within the basic linker (Geyer et al., 2018; Widlund et al., 2011). However, it is difficult to reconcile the idea that neutralizing only two positive charges (Stu2$^{KR/AA}$), would result in comparable defects to deleting the entire basic linker (Stu2$^{\Delta BL}$). We modified a previously developed in vitro whole cell lysate assay (Bergman et al., 2019) to examine how these Stu2 variants impact microtubule dynamics. Cells with the *stu2-AID* system and expressing GFP-Tub1 (to visualize microtubules) were arrested in metaphase using a temperature sensitive *cdc23-1* allele (a component of the anaphase promoting complex). Whole cell lysate was isolated from these cells, the lysate was subsequently incubated with fluorescently labeled microtubule seeds, and microtubule dynamics were observed by TIRF microscopy (Fig. 2C and Fig. S2B-E). As expected, we observe that in lysate containing Stu2^{WT} compared to lysate depleted of Stu2 there was a significant increase in the microtubule assembly rate (Stu2^{WT}, 0.396 ± 0.014 µm/min; Stu2 depleted, 0.192 ± 0.015 µm/min). In lysate containing Stu2$^{\Delta BL}$ there was a substantial decrease in the elongation rates of microtubules (0.198 ± 0.012 µm/min), which was nearly indistinguishable from Stu2 depletion conditions, consistent with the importance of the basic linker domain in microtubule polymerase function (Geyer et al., 2018; Widlund et al.,

2011). However, in Stu2$^{KR/AA}$ and Stu2$^{\Delta 592-606}$-containing lysates, the microtubule assembly rates were comparable to Stu2^{WT} (0.411 ± 0.022 µm/min and 0.467 ± 0.022 µm/min; Fig. 2C).

We also used an in vitro microtubule polymerase assay with recombinant Stu2 and purified yeast tubulin (Ayaz et al., 2014; Geyer et al., 2018), and found that the addition of Stu2$^{KR/AA}$ stimulated microtubule growth rates, albeit to a slightly lesser extent than Stu2^{WT} in this context (growth rate 1.878 ± 0.105 µm/min and 2.268 ± 0.068 µm/min, respectively; Fig. 2D). This slight decrease is not surprising given the correlation between degree of positive charge of the basic region and microtubule polymerase activity previously observed in this assay (Geyer et al., 2018). Furthermore, this decrease is not large enough to explain the defects in cell viability observed in *stu2$^{KR/AA}$* mutants: we previously showed that *stu2* mutants with TOG1 or TOG2 inactivated have an even greater decrease in polymerase activity and yet display no viability defect (Geyer et al., 2018).

Next, we hypothesized that an increase in the rate of microtubule disassembly in cells expressing Stu2$^{\Delta BL}$, Stu2$^{\Delta 592-606}$, and Stu2$^{KR/AA}$ could account for the short spindle phenotype that we observed in these cells. Here, we observed that Stu2 plays a role in accelerating the disassembly of microtubules: the disassembly rate in Stu2^{WT} lysate (0.797 ± 0.024 µm/min) was significantly greater than in lysate with Stu2 depleted (0.471 ± 0.049 µm/min). Whereas Stu2 lacking the entire basic region cannot promote fast microtubule disassembly (Stu2$^{\Delta BL}$, disassembly rate 0.471 ± 0.074 µm/min), Stu2 variants with smaller deletions remain competent to promote fast microtubule disassembly (Stu2$^{\Delta 592-606}$, 0.820 ± 0.023 µm/min; Stu2$^{KR/AA}$, 0.777 ± 0.024 µm/min) (Fig. 2C). These differences mirror what we observed for polymerization. Together, these results show that Stu2 not only accelerates microtubule growth but also accelerates microtubule disassembly, and these activities depend on Stu2's basic linker. However, these activities do not depend on the conserved patch of residues within Stu2's basic linker. Thus, the short spindle phenotype observed in cells expressing Stu2$^{\Delta 592-606}$ or Stu2$^{KR/AA}$ cannot be explained by alterations in Stu2's ability to stimulate microtubule assembly or disassembly (Fig. S2C-F), which motivated us to explore other mitotic defects associated with *stu2$^{KR/AA}$* mutants to help give insight into the functional importance of these two residues.

stu2$^{KR/AA}$ expressing cells display pleiotropic mitotic defects.

To identify other mitotic defects of *stu2$^{KR/AA}$* mutants, cells with the *stu2-AID* system and expressing Spc110-mCherry were arrested in metaphase using a *cdc20-AID* allele. Additionally, strains harbored a copy of Mtw1-GFP to visualize kinetochores. *stu2$^{KR/AA}$* cells display pleiotropic mitotic defects (Fig. 2E), including a significantly greater portion of cells with a mono-lobed kinetochore cluster (*stu2$^{KR/AA}$* 28% vs *STU2^{WT}* 1%), spindle orientation defects (i.e. mitotic spindle positioned at an angle greater than 45 degrees relative to the bud axis; *stu2$^{KR/AA}$* 29% vs *STU2^{WT}* 17%), and detached kinetochores (i.e. Mtw1-GFP signal isolated from the inter-spindle GFP clusters; *stu2$^{KR/AA}$* 40% vs *STU2^{WT}* 2%). These pleiotropic defects observed in *stu2$^{KR/AA}$* expressing cells suggest that Stu2$^{K598\ R599}$ play a crucial role in multiple of Stu2's functions.

Stu2$^{K598\ R599}$ are required for Stu2's ability to localize to the nucleus.

Many fungal species undergo a closed mitosis and require the import of MAPs into the nucleus to accomplish their mitotic functions. This process involves interactions between the α-subunit of the importin complex (Kap60 in *S. cerevisiae*) and the nuclear localization sequence (NLS) of proteins to be imported. The β-subunit of the importin complex (Kap95) interacts with the nuclear pore complex facilitating transport of the trimer into the nucleus (Christie et al., 2016; Enenkel et al., 1995). We hypothesized that one way to explain the pleiotropic mitotic defects observed in *stu2$^{KR/AA}$* mutants would be if the mutations altered Stu2's ability to properly localize to the nucleus during mitosis. The idea that Stu2$^{K598\ R599}$ are part of Stu2's NLS is somewhat consistent with work from Kosugi *et al.* who defined a nuclear localization sequence (NLS) class with the consensus sequence (P/R)XXKR(^DE)(K/R), where (^DE) indicates any residue except for D/E (Kosugi et al., 2009). Stu2$^{592-606}$ contains the sequence P-S-K-R-V where the proline, lysine, and arginine are important for full viability (Fig. 1C and Fig. S1D). Although, this sequence in Stu2 does not precisely fit the described consensus NLS class we still considered that this could represent Stu2's NLS.

To test this hypothesis, we compared Stu2-GFP nuclear localization in cells expressing Stu2^{WT} vs Stu2$^{KR/AA}$. Cells with the *stu2-AID* system were arrested in metaphase using a *cdc20-AID* allele, and the nuclear envelope was fluorescently labeled by tagging the nucleoporin protein, Nup2, with mKate. We observed that Stu2^{WT} expressing cells form two adjacent, discrete GFP puncta within the nucleus, which previous work showed was proximal or kinetochore-associated (Humphrey et al., 2018; Miller et al., 2019; Zahm et al., 2021). Stu2$^{KR/AA}$ formed similar puncta, although the puncta were less fluorescently intense, and there were additional, distal GFP puncta within the cell (Fig. 3A). There also appeared to be noticeably increased GFP signal in the cytoplasm with Stu2$^{KR/AA}$ compared to Stu2^{WT} expressing cells. We quantified the ratio of nuclear to cytoplasmic Stu2-GFP intensity, and found substantially less nuclear localization in cells expressing Stu2$^{KR/AA}$ (nuclear to cytoplasmic GFP ratio: 0.59 ± 0.03) compared to Stu2^{WT} (1.57 ± 0.03), suggesting significantly disrupted nuclear localization of this mutant protein (Fig. 3A).

To further test if Stu2$^{K598\ R599}$ are important residues in Stu2's nuclear localization sequence (NLS) we examined the ability of Stu2$^{KR/AA}$ to interact with the α-subunit of the importin complex, Kap60, which binds directly to the NLS of nuclear localization sequence-containing proteins (Christie et al., 2016; Enenkel et al., 1995). We tagged Kap60 with a Flag epitope and used α-Flag conjugated magnetic beads to pulldown Kap60 and examine binding of V5-tagged Stu2^{WT} or Stu2$^{KR/AA}$. Here we observe that the co-immunopurified Stu2$^{KR/AA}$-V5 signal was significantly reduced compared to the signal for Stu2^{WT}-V5, suggesting that Stu2$^{K598\ R599}$ are important for binding to Kap60 and promoting Stu2's import into the nucleus (Fig. 3B).

Since Stu2$^{K598\ R599}$ are necessary for nuclear localization, we next wanted to assess if Stu2's conserved patch in the basic linker, Stu2$^{592-607}$, is sufficient to drive nuclear localization. We engineered a fusion protein containing Stu2's conserved patch fused to GFP-GST to determine if Stu2$^{592-607}$ is sufficient to localize GFP to the nucleus. The GST protein was included to make the protein construct large enough to limit the amount of GFP freely diffusing

into the nucleus (Okada et al., 2014). We used Nup2-mKate to fluorescently mark the nucleus, and arrested cells in metaphase in the presence of auxin again using a *cdc20-AID* allele. We ectopically expressed GFP-GST constructs under the Stu2 promoter. When examined, GFP-GST alone primarily localized to the cytoplasm (nuclear to cytoplasmic GFP signal ratio of 0.79 ± 0.03). The nuclear pool of this construct suggests that some GFP-GST was able to freely diffuse into the nucleus. As a positive control, we fused GFP-GST with NLS^{SV40}, the NLS of the SV40 virus large T-antigen protein. As expected, the addition of NLS^{SV40} promoted GFP nuclear import (nuclear to cytoplasmic GFP signal ratio of 2.05 ± 0.04). Importantly, fusion of $Stu2^{592-607}$ to GFP-GST was sufficient to promote nuclear import, and this activity was disrupted when the $Stu2^{K598\ R599}$ residues were mutated in this minimal context (nuclear to cytoplasmic ratio of GFP signal of 1.49 ± 0.04 for $Stu2^{592-607}$-GFP-GST and 0.82 ± 0.03 for $Stu2^{592-607(KR/AA)}$-GFP-GST; Fig. 3C and Fig. S3). These results indicate that Stu2's conserved patch within its basic linker region is sufficient to promote nuclear import, and this activity is dependent on $Stu2^{K598\ R599}$.

Stu2's nuclear import is promoted during mitosis, likely through CDK phosphorylation of S603.

We next wanted to determine if Stu2's nuclear import is regulated throughout the cell cycle. Stu2 has important nuclear-specific functions during mitosis (Humphrey et al., 2018; Miller et al., 2016, 2019; Severin et al., 2001; Zahm et al., 2021), but it also has cellular functions in the cytoplasm, especially in G1 (Gunzelmann et al., 2018; van der Vaart et al., 2017). We hypothesized that nuclear levels of $Stu2^{WT}$ would increase between G1 and mitosis. To examine this, we arrested cells either in G1 or metaphase of mitosis, by treatment with α-factor or by depleting Cdc20-AID with auxin, respectively. We used Nup2-mKate to visualize the nucleus and examined the ratio of nuclear to cytoplasmic $Stu2^{WT}$-GFP. We observed a significant increase in the ratio of nuclear to cytoplasmic $Stu2^{WT}$-GFP between G1 and mitosis (1.14 ± 0.03 in G1 vs 1.48 ± 0.03 in mitosis, Fig. 4A). This was also the case when we examined the minimal $Stu2^{592-607}$-GFP-GST construct (Fig. S4A), suggesting nuclear localization is regulated in part by a regulatory sequence within $Stu2^{592-607}$ which functions to promote mitosis-specific nuclear localization of Stu2.

We next considered which element within Stu2's conserved patch is responsible for Stu2's mitotic-specific nuclear localization. Stu2's conserved patch contains a consensus CDK phosphorylation site (S603), which multiple studies have identified as being phosphorylated in vitro and in vivo (Albuquerque et al., 2008; Holt et al., 2009; Lanz et al., 2021; MacGilvray et al., 2020; Okada et al., 2014; Swaney et al., 2013). This observation, coupled with the fact that phosphorylation can promote the nuclear localization activity of some NLS sequences (Faustova et al., 2022; Jans et al., 2000; Nardozzi et al., 2010), raised the possibility that phosphorylation of S603 was a mechanism to regulate Stu2's nuclear import. To examine this, we made a phosphorylation deficient mutant (S603A). As before, we used the *stu2-AID* system, Nup2-mKate to fluorescently mark the nucleus, and arrested cells either in G1 or mitosis. We observed similar ratios of nuclear to cytoplasmic GFP intensities in G1 between $Stu2^{WT}$ (1.14 ± 0.03) and $Stu2^{S603A}$ (1.05 ± 0.03) expressing cells. In contrast, the mitotic increase in nuclear to cytoplasmic Stu2-GFP intensities observed with $Stu2^{WT}$, was completely

abolished in Stu2^{S603A} (1.48 ± 0.03 in Stu2^{WT} vs 0.97 ± 0.03 in Stu2^{S603A}; Fig. 4A). Similar effects were observed in the minimal Stu2$^{592-607}$-GFP-GST construct where mutational effects were isolated from Stu2's NES function (van der Vaart et al., 2017). In this minimal context, Stu2$^{592-607(S603A)}$-GFP-GST displayed significantly reduced nuclear GFP localization compared to Stu2$^{592-607}$-GFP-GST in metaphase arrested cells (0.81 ± 0.03 for Stu2$^{592-607(S603A)}$-GFP-GST vs 1.49 ± 0.04 for Stu2$^{592-607}$-GFP-GST). We also examined a phosphorylation mimicking construct, Stu2$^{592-607(S603E)}$-GFP-GST, and found an increased nuclear to cytoplasmic ratio relative to the phosphonull Stu2$^{592-607(S603A)}$-GFP-GST (Fig. S4B). However, not too surprisingly, the nuclear to cytoplasmic ratio of GFP intensities of cells expressing this phosphorylation mimicking construct was significantly less than those cells expressing Stu2$^{592-607}$ suggesting that the glutamic acid used to mimic phosphorylation was not as effective at promoting nuclear localization as what we expect to be a phosphorylated serine seen in cells expressing the wild-type sequence (Fig. S4A-B). Taken together, these findings suggest that CDK phosphorylation of S603 promotes Stu2's import into the nucleus as cells enter mitosis (Fig. 4B).

The primary and essential function of the basic linker is to localize Stu2 to the nucleus. We next hypothesized that if decreased nuclear localization was responsible for the viability defects we see in *stu2$^{KR/AA}$* mutants, we could potentially rescue these defects by modulating the nuclear ratio of Stu2$^{KR/AA}$. To address this, we asked if a fusion with NLS^{SV40} would rescue the *stu2$^{KR/AA}$* viability defect. Fusing NLS^{SV40} to Stu2^{WT} resulted in similar growth as Stu2^{WT} expressing cells. Intriguingly, the *stu2$^{KR/AA}$* growth and nuclear localization defects were completely rescued when fused with NLS^{SV40} (Fig. 5A-B). We observed similar results by modulating Stu2 nuclear export by the previously described phospho-regulation of Stu2's NES (van der Vaart et al., 2017). Briefly, Stu2's NES is regulated via Sch9-dependent phosphorylation of Stu2$^{S813\ S815}$, to promote Stu2's nuclear export. When we combined *stu2$^{KR/AA}$* with phosphorylation mimicking mutants (S813D S815D), thus decreasing the nuclear pool of Stu2 by promoting nuclear export, we observe an exacerbation of the viability defects seen in *stu2$^{KR/AA}$* expressing cells (Fig. S5A-B). Conversely, when we increased the nuclear pool of Stu2$^{KR/AA}$ by combining with the phosphorylation deficient mutations (S813A S815A), thus inhibiting Stu2 nuclear export, we observe a partial rescue of the *stu2$^{KR/AA}$* viability phenotype. Together, these results indicate that Stu2's nuclear localization is critical for cell viability, and furthermore, the predominant function of Stu2$^{K598\ R599}$ is to promote Stu2's import into the nucleus.

Stu2's entire basic linker (Stu2^{BL}) is an essential domain and implicated in many of its microtubule regulatory functions (Geyer et al., 2018; Gunzelmann et al., 2018; Herman et al., 2020; Miller et al., 2019; Wang & Huffaker, 1997). For example, we observed that Stu2's ability to increase rates of microtubule polymerization, depolymerization, and catastrophe depend on the basic linker domain (Fig. 2C and Fig. S2C-E). On the other hand, our results thus far open the possibility that the essential function contained within the basic linker domain is to localize Stu2 to the nucleus. To test this hypothesis, we asked if restoring nuclear localization could rescue cell viability in *stu2* mutants in which the entire basic linker is deleted. Remarkably, this appeared to be the case. We observed that the viability defects of deleting

Stu2's entire basic linker (Stu2$^{\Delta BL}$) could be rescued by fusing with NLS^{SV40} (Fig. 5C and Fig. S5C). We additionally examined the viability of *stu2$^{\Delta BL}$-NLS^{SV40}* expressing cells in the presence of low concentrations of a microtubule poison, benomyl, to further examine if any region of the basic linker is required for viability when cells are challenged. Here we see that *stu2$^{\Delta BL}$-NLS^{SV40}* expressing cells are sensitive to benomyl compared to *STU2^{WT}-NLS^{SV40}* cells. Interestingly, this benomyl sensitivity was rescued when we added-back the conserved patch to this construct (i.e. *stu2$^{\Delta BL::592-606}$-NLS^{SV40}*; Fig. 5C). These results indicate that the Stu2$^{592-606}$ conserved patch, in addition to its nuclear localization activity, carries out a function that is required when the cells are challenged with benomyl. However, our findings suggest that the predominant and essential function of the basic linker region is to localize Stu2 to the nucleus.

Anaphase spindle elongation rates, but not metaphase spindle length, correlates with Stu2 microtubule polymerase function.

Our findings up until this point suggest that i) nuclear Stu2 is required to build a mitotic spindle (Fig. 2B and Fig. S2A); ii) the predominant function of Stu2^{BL} is to localize Stu2 to the nucleus (Fig. 5C); and iii) Stu2^{BL} is required for Stu2's ability to polymerize and depolymerize microtubules in vitro (Fig. 2C-D). Considering these observations, we examined whether Stu2's microtubule polymerization and depolymerization activities are required to form a normal length mitotic spindle. To examine this, we observed the spindle length in cells expressing *stu2$^{\Delta BL}$-NLS^{SV40}* to determine if this mutant, which is defective in stimulating microtubule assembly and disassembly in vitro (Fig. S5D-F), can form a normal length metaphase spindle. As before, we used the *stu2-AID* system, arrested cells in metaphase using a *cdc20-AID* allele, and visualized the spindle pole bodies using Spc110-mCherry. As previously observed, cells expressing *stu2$^{\Delta BL}$* had a significantly shorter mitotic spindle length when compared to *STU2^{WT}* expressing cells. In cells expressing *STU2^{WT}-NLS^{SV40}* the average mitotic spindle length was similar to *STU2^{WT}* expressing cells. Intriguingly, in cells expressing *stu2$^{\Delta BL}$-NLS^{SV40}* the spindle length was comparable to cells expressing *STU2^{WT}* (Fig. 5D). These findings demonstrate that Stu2's nuclear microtubule polymerase activity does not correlate with the ability to form a normal metaphase spindle, and implies that an additional nuclear function of Stu2, which is independent of its basic linker-dependent microtubule lattice binding, is required to form a normal mitotic spindle.

Finally, we examined the ability of cells expressing *stu2$^{\Delta BL}$-NLS^{SV40}* to elongate their anaphase spindle with normal kinetics. We hypothesized that if the microtubule polymerase activity of Stu2$^{\Delta BL}$ is disrupted in vivo, then the rate at which the mitotic spindle is elongated during anaphase would be decreased (Severin et al., 2001). To examine this, we used cells with the *stu2-AID* system, and expressing Spc110-mCherry. We used live-cell imaging of asynchronously growing cells treated with auxin (to degrade endogenous Stu2-AID), and measured the mitotic spindle length of cells every minute as they progressed into and through anaphase (Fig. 5E). Consistent with our observations of cells arrested in metaphase (Fig. 5D), we see that the mitotic spindle length prior to anaphase onset is similar when comparing cells expressing *stu2$^{\Delta BL}$-NLS^{SV40}* versus *STU2^{WT}-NLS^{SV40}* (Fig. 5F). However, the rate at which *stu2$^{\Delta BL}$-NLS^{SV40}* cells elongated their spindle during anaphase was significantly reduced compared to cells expressing *STU2^{WT}-NLS^{SV40}* (Fig. 5F). This result provides evidence that

Stu2's basic linker is required in vivo to properly elongate the mitotic spindle during anaphase, likely acting as a microtubule polymerase to carry out this function. It also suggests that the rapid elongation of the mitotic spindle during anaphase is not critical for cell viability. Taken together, our findings suggest that Stu2 activity is required in the nucleus to form a normal mitotic spindle, but given that these functions are independent of basic linker-dependent microtubule lattice binding, this essential function(s) is likely independent of its ability to stimulate microtubule growth.

DISCUSSION

Previous work demonstrated that the TOG family of proteins, including budding yeast homolog Stu2, function as critical regulators of microtubules, including controlling microtubule polymerization, depolymerization, nucleation, and in regulating kinetochore-microtubule interactions (Ayaz et al., 2014; Brouhard et al., 2008; Chen et al., 1998; Geyer et al., 2018; Humphrey et al., 2018; King et al., 2020, 2021; Kinoshita et al., 2002; Kosco et al., 2001; Miller et al., 2016; Podolski et al., 2014; Severin et al., 2001; Wang & Huffaker, 1997; Widlund et al., 2011). These described microtubule regulatory functions depend on two microtubule binding elements that are conserved within all TOG family members: TOG domain arrays that to bind to $\alpha\beta$-tubulin dimers, and a basic linker domain important for binding the microtubule lattice. The findings reported here show that while the basic linker domain is required for Stu2's ability to stimulate microtubule assembly and disassembly in vitro, surprisingly, the only essential function contained within this domain is to promote Stu2's nuclear import. Thus, Stu2 carries out an activity in the nucleus that is essential for cell viability. However, our findings reveal that its required function there appears distinct from its ability to bind to the microtubule lattice, and stimulate large changes in tubulin subunit addition or loss to microtubule tips. These observations have important implications for the function of the TOG family of proteins, and how they work to carry out their essential activities.

Stu2's nuclear import and function is regulated

In this study we identify a conserved patch of amino acids within Stu2's basic linker region, Stu2$^{592\text{-}607}$, that is necessary and sufficient for directing nuclear localization. We find that two positive residues within this region, Stu2$^{K598\ R599}$, are required and that mutation of these residues impairs nuclear localization by disrupting interactions with the importin complex. Furthermore, restoring nuclear localization of this *stu2*$^{KR/AA}$ mutant by fusing with the SV40^{NLS} rescues the mitotic defects observed. We also observed cell cycle-dependent regulation of nuclear import contained within this conserved patch. Considering numerous prior studies find that Stu2^{S603} is phosphorylated by CDK both in vitro and in vivo (Albuquerque et al., 2008; Holt et al., 2009; Lanz et al., 2021; MacGilvray et al., 2020; Okada et al., 2014; Swaney et al., 2013), that preventing phosphorylation of this site (Stu2^{S603A}) disrupts the increase in mitotic nuclear localization, and that mimicking phosphorylation (Stu2^{S603E}) results in a greater nuclear localization compared to the phosphorylation deficient mutant, we propose that phosphorylation of this residue is a likely mechanism by which Stu2's nuclear localization is promoted during mitosis. A confounding observation is the apparent disconnect between the degree to which various *stu2* mutants affect nuclear localization and their associated growth phenotypes. We observe that *stu2*$^{KR/AA}$ mutants, which we show significantly disrupt Stu2's nuclear localization, display substantial growth defects (Fig. 1C, Fig. 3A, and Fig. S1). This is in contrast to the CDK phosphorylation deficient mutant where, despite an apparently similar defect in nuclear localization as *stu2*$^{KR/AA}$ (judged by quantifying the ratio of the nuclear to cytoplasmic GFP signal intensities; Fig. S4B), the *stu2*^{S603A} mutants have no perceptible growth defect (Fig. 1C and Fig. S1D), even when combined with phosphorylation mimicking mutants (S813D S815D) that presumably further decrease the nuclear pool of Stu2 by promoting nuclear export (data not shown). These discrepancies suggest that either our

fluorescent microscopy-based assay for examining Stu2's nuclear localization is not sensitive enough to pick up on slight but important differences in nuclear Stu2 levels, or that Stu2's nuclear-to-cytoplasmic levels are subject to more complicated regulation. Regardless, our work reveals that insufficient nuclear Stu2 leads to pleiotropic mitotic defects. Future work will be required to determine the exact levels of nuclear Stu2 required to support cell viability.

Stu2 carries out an essential nuclear function that does not require basic linker-dependent microtubule lattice binding

Stu2 is known to carry out numerous functions in the cell, and to our knowledge, the basic linker domain has been implicated in each of these previously described activities. The best described function of the basic linker is with respect to its microtubule polymerase function. Across multiple TOG protein family members, the ability to stimulate microtubule polymerization depends on the presence of a basic region, and the polymerization activity correlates with the number of positive residues within these domains (Geyer et al., 2018; Widlund et al., 2011; Fig. 2C-D, Fig. 5E-F). In this context, the basic region is proposed to bind the microtubule lattice, either allowing Stu2 to more effectively target the microtubule end via diffusion (Widlund et al., 2011), and/or facilitating a ratcheting 'processivity' mechanism, via an observed antagonism of basic linker-dependent lattice binding by TOG domains when engaged with tubulin (Geyer et al., 2018). In addition to these functions, nucleation of microtubules through γ-TuSC oligomerization (Gunzelmann et al., 2018), and Stu2/chTOG's kinetochore function (Herman et al., 2020; Miller et al., 2019), all depend on the presence of either specific residues within, or the entire basic linker domain. Collectively, these observations make our findings all the more surprising that, beyond promoting nuclear localization, the basic linker is largely dispensable for cell viability. An important remaining question is what principal activity does Stu2 carry out in the nucleus, that does not require its basic linker-dependent activities? It is possible that microtubule lattice binding is dispensable because some other protein/factor positions Stu2 at the microtubule tip, where it can carry out its function. However, our observations that the basic linker is required for Stu2's microtubule regulatory functions, both in vitro using a whole cell lysate assay where other factors are present (Fig. 2C-D), and in cells (Fig. 5E-F), suggests this is not the case. It is also possible that Stu2 is required at microtubule ends to either bind and alter tubulin dimer conformation, microtubule transition frequencies, microtubule nucleation, or small-scale addition/subtraction of tubulin dimers. These activities presumably would depend on TOG domains interacting with αβ-tubulin dimers, and not on basic linker-dependent lattice binding. Future work determining which portions of Stu2 are required for this essential nuclear activity will be an important step in determining what essential function Stu2 carries out in the cell's nucleus. Regardless, our findings here strongly suggest that the essential function of Stu2 is not the ability to stimulate large changes in the addition or loss of tubulin subunits to the end of a microtubule.

Conserved patch within basic linker may have additional functions

While the predominant function carried out by the conserved patch within Stu2's basic linker is nuclear localization, we found that cells with restored nuclear localization but lacking the basic linker (i.e. *stu2*$^{\Delta BL}$-*NLS*^{SV40}) displayed growth defects when challenged by the microtubule poison, benomyl. Interestingly, this benomyl sensitivity was rescued when only

the conserved patch of amino acids, Stu2$^{592-606}$, is added-back to this construct (i.e. *stu2*$^{\Delta BL::592-606)}$*-NLS*^{SV40}; Fig. 5C). Adding these 15 amino acids alone is unlikely to restore the number of basic residues required for microtubule polymerase function (Geyer et al., 2018). These findings suggest that, in addition to localizing Stu2 to the nucleus, this conserved patch is required for another function of Stu2. Given that these exact residues have been implicated in Stu2's ability to regulate kinetochore-microtubule attachments (Herman et al., 2020), we favor the idea that this additional function is related to Stu2's kinetochore activities.

This mechanism may involve direct contacts between Stu2$^{592-606}$ and the Ndc80 complex, which directly interact via cross-linking mass spectrometry (Miller et al., 2019). Alternatively, importin complex binding may serve as a mechanism to regulate Stu2 function, perhaps via directly restricting activity or constraining binding partners. This mechanism may be a more general means to regulate the activity of MAP proteins. For example, importin binding controls the efficiency of microtubule nucleation by TPX2 via selectively blocking the interaction with microtubule nucleation intermediates (Roostalu et al., 2015). Additionally, a recent study by Shrestha *et al.* found that importin α/β binding to the microtubule destabilizing Kinesin-8, Kif18B, directly regulates its ability to control microtubule dynamics and spindle positioning by altering its binding to the microtubule lattice (Shrestha et al., 2022). An importin complex association may even regulate MAP function upon nuclear envelope breakdown (i.e. in mitosis of higher eukaryotes), where a Ran-GDP/GTP gradient still exists with Ran-GTP being the predominant species adjacent to the chromosomes. This biochemical barrier facilitates spatial regulation of protein activity, and accurate formation of the mitotic spindle (Caudron et al., 2005; Clarke & Zhang, 2008; Dasso, 2001; Kalab et al., 2002; Kaláb et al., 2006; Kalab & Heald, 2008). Considering these observations, it is possible that importin complex binding to chTOG, after nuclear envelope breakdown, can serve to regulate other binding interactions, for example with the Ndc80 complex. This possibility could reconcile the observations made here, and those we previously made in which analogous mutations to the conserved patch in chTOG's basic linker domain, disrupt its ability to correct erroneous kinetochore-microtubule attachments (Herman et al., 2020). The observations made here provide critical tools to examine these hypotheses.

Conclusions

Ultimately, our findings suggest that despite microtubule polymerase and depolymerase activity being the canonical function of the TOG family of proteins, the ability of Stu2 to stimulate large addition or subtraction of tubulin subunits to microtubule tips is dispensable for cell viability. While it is not clear what the essential function is at present, it will be important future work to understand what basic linker-independent activities TOG family members can perform. This work will have significant implications for our understanding of how this conserved family of proteins work to accomplish their essential functions.

ACKNOWLEDGEMENTS

The authors declare no competing financial interests. We thank Sue Biggins, Trisha Davis, Eris Duro and Adèle Marston for reagents; Sue Biggins, Jake Herman, Trisha Davis and the Miller lab for critical reading of the manuscript. This work was supported by funds from the Judy Chandler Webb Endowed Chair in the Biological Sciences (to G.B), Robert A Welch Foundation I-1901 (to L.R.), 5 For the Fight (to M.P.M), Pew Biomedical Scholars (to M.P.M), and NIH grants R01GM098542 (to L.R.), R01GM47842 (to G.B.), and R35GM142749 (to M.P.M).

METHODS

Yeast strains and plasmids

Saccharomyces cerevisiae strains used in this study are described in Table S1 and are derivatives of M3 (W303) or M1652 (S288C). Standard media and microbial techniques were used (Sherman et al., 1974). Yeast strains were constructed by standard genetic techniques. *NUP2-mKATE2* and *KAP60-3FLAG* were constructed by PCR-based methods (Longtine et al., 1998). Strains containing previously described alleles were also generously provided (*cdc20-IAA17* from Eris Duro and Adèle Marston, *MTW1-3GFP* from Sue Biggins, *GFP-TUB1* and *cdc23-1* from Georjana Barnes and David Drubin, and *SPC110-mCherry* from Trisha Davis). *stu2-3HA-IAA7*, *pGPD1-OsTIR1* and *pSTU2-STU2-3V5* are described in (Miller et al., 2016). *STU2-3V5* variants were constructed by mutagenizing pM225 as described in (Liu & Naismith, 2008; Tseng et al., 2008). *STU2-Halo-3V5* variants were constructed by mutagenizing pM630 as described in (Liu & Naismith, 2008; Tseng et al., 2008). *pSTU2-STU2-GFP* is described in (Miller et al., 2019). *STU2-GFP* variants were constructed by mutagenizing pM488 as described in (Liu & Naismith, 2008; Tseng et al., 2008). *stu2*$^{592\text{-}607}$*-GFP-GST* variants were constructed by mutagenizing pM774 as described in (Liu & Naismith, 2008; Tseng et al., 2008). Plasmids and primers used in their construction are listed in Table S2 and further details of plasmid construction including plasmid maps are available upon request.

Auxin inducible degradation

The auxin inducible degron (AID) system was used as described (Nishimura et al., 2009). Cells expressed C-terminal fusions of the protein of interest to an auxin responsive protein (IAA7) at the endogenous locus. Cells also expressed TIR1, which is required for auxin-induced degradation. 500 µM auxin (indole-3-acetic acid; Sigma-Aldrich) dissolved in DMSO was added to liquid media or top-plated on agar to induce degradation of the AID-tagged protein. Auxin was added to liquid media 2 hours prior to harvesting cells when arresting cells in mitosis or otherwise 30 minutes prior to harvesting.

Spot viability assay

For the spot viability assay, the desired strains were grown overnight on YPD plates containing yeast extract peptone plus 2% glucose (YPD) medium. The following day, approximately equal amounts of each desired strain was used for a 1:5 dilution series and was spotted on YPD+DMSO, YPD+500 µM auxin, YPD+DMSO+6.5µg/mL benomyl, or YPD+500 µM auxin+6.5µg/mL benomyl plates. Plates were incubated at 23°C for 2–3 days.

Cell Fixation, Imaging conditions, and Image Analysis

Exponentially growing cultures were treated with 500 µM auxin for 2h prior to harvesting when arresting cells in mitosis or 30 minutes prior to harvesting when arresting cells in G1 (Miller et al., 2016), then fixed (see below) and analyzed for Stu2-GFP localization and Nup2-mKATE localization or Mtw1-GFP distribution and spindle length and orientation (Spc110-mCherry). For each strain an aliquot of cells was fixed with 3.7% formaldehyde in 100mM phosphate

buffer (pH 6.4) for 1 min. Cells were washed once with 100mM phosphate (pH 6.4), resuspended in 100mM phosphate, 1.2M sorbitol buffer (pH 7.5) and permeabilized with 1% Triton X-100 stained with 1 µg/ml DAPI (4', 6-diamidino-2-phenylindole; Molecular Probes). Cells were imaged using a DeltaVision Ultra microscope with a 60X objective (NA = 1.42), equipped with a sCMOS digital camera. Twenty-one Z-stacks (0.2 micron apart) were acquired, and all frames were deconvolved using standard settings. For quantification of nuclear localization image stacks were projected using the average intensity. For observation of Mtw1-GFP or Spc110-mCherry image stacks were maximally projected. softWoRx image processing software was used for image acquisition and processing.

A software was developed to automate the analysis of cellular GFP localization as well as spindle lengths. DIC images were sent into cell segmentation model to segment individual cells. For this implementation, the model developed by [https://github.com/alexxijielu/yeast_segmentation], which uses Mask-RCNN Segmentation [https://arxiv.org/pdf/1703.06870.pdf], was used; however, due to the modular nature of the software, any segmentation model could be easily used. After the objects (i.e. individual mother and daughter cells) have been individually segmented, mother-daughter pairs are merged together by calculating the nearest neighbor of each object within 3 pixels. If the nearest neighbor of object A is object B, and the nearest neighbor of object B is object A, then the two objects are merged as a single mother-daughter pair, representing a large-budded cell, otherwise the cells are ignored during further analysis. Segmented cells that were improperly segmented were manually ignored. Once the large-budded cells have been detected in the DIC image, the outlines of those large-budded cells are used to extract the location of each cell in the mCherry/mKATE and GFP images.

The spindle length is calculated by first identifying the locations of high intensity Spc110-mCherry signal for a given large-budded cell. This is accomplished by converting the mCherry image for a given cell to grayscale, smoothing the image with a Gaussian blur (kernel size of (3,3) and kernel standard deviation of 1 along both the x and y axes) then cleaning the noise from the image by using an adaptive Gaussian threshold with Otsu binarization. Next, contours in the image are detected and the two largest contours are extracted. To determine the spindle length the moment of each contour is calculated, and then the center of each contour is calculated from the moment. This center point represents the spindle pole body in the Spc110-mCherry images. The spindle line is then calculated as the line between the center of each contour. Length of this spindle line is calculated and represents the spindle length.

To calculate the nuclear and cytoplasmic GFP intensities, the contours of the high intensity Nup2-mKATE signal, representing the nucleus, is determined as described above (similar to determining the contours of the Spc110-mCherry signal). Next, the background data is removed from the GFP image by using a rolling ball background subtraction algorithm with a radius of 50. The nuclear GFP intensity is then determined by adding the intensity values from each point in the GFP image that falls within the nucleus contour determined earlier in this process. The final step is to calculate the cellular intensity. Similar to the previous process, the GFP image is converted to grayscale, smoothed with a Gaussian blur (kernel size of (13,

13) and kernel standard deviation of 5 in both the x and y axes), and cleaned using an adaptive Gaussian threshold with Otsu binarization. Contours are then extracted from the image. The cellular GFP intensity is then calculated by extracting the intensity values of every point within the cellular contour. Cytoplasmic GFP intensity is calculated by subtracting the nuclear GFP intensity from the cellular GFP intensity.

To analyze spindle orientation and Mtw1-GFP distribution projected images were imported into FIJI for manual analysis. To determine spindle orientation the angle tool was used to measure the angle between the spindle axis (a line between the two Spc110-mCherry puncta) and the mother-daughter bud axis (a line between the center of the distal ends of the large-budded cell). Values were reported as less than or greater than 45 degrees. To determine if a cell had a bi-lobed versus mono-lobed kinetochore cluster, Mtw1-GFP signals were examined. A mono-lobed kinetochore cluster was identified as a Mtw1-GFP puncta that could not be distinguished into two separate punctae whereas bi-lobed kinetochore clusters had two distinguishable Mtw1-GFP punctae. Cells belonging to each group were counted and represented as a proportion for each strain. To determine if a cell had a detached kinetochore, Mtw1-GFP signals were examined. A detached kinetochore cluster was identified as a Mtw1-GFP puncta that was dimmer and distinct from the intra-spindle Mtw1-GFP signal. Cells belonging to this group versus cells with no detached kinetochores were counted and represented as a proportion for each strain.

Live cell imaging conditions and analysis

Exponentially growing cultures, grown in synthetic complete media, were treated with 500 μM auxin 30 min prior to harvesting to degrade Stu2-AID and analyzed for Stu2-GFP (ectopically expressed, *STU2^{WT}-GFP* or *stu2$^{\Delta BL}$-GFP*) distribution and spindle length. For each strain an aliquot of cells was pelleted and resuspended in a volume of synthetic complete media with 500 μM auxin to optimize cell density for imaging (OD_{600}≈5). Cells were adhered to a coverslip coated in Concanavalin A as described in (Fees et al., 2017) and the chamber was sealed using petroleum jelly. Cells were imaged using a DeltaVision Ultra microscope with a 60X objective (NA = 1.42), equipped with a sCMOS digital camera. Images of the Spc110-mCherry signal, Stu2-GFP signal and DIC were acquired through the thickness of the cells using Z-stacks 0.3 micron apart. These images were acquired every 1 minute. All frames were deconvolved using standard settings. Image stacks were maximally projected for analysis of spindle lengths and Stu2 distribution. softWoRx image processing software was used for image acquisition and processing.

Projected images were imported into FIJI for analysis. Background signal was subtracted and in cells undergoing spindle elongation the distance between Spc110-mCherry punctae were measured every minute beginning 5 minutes prior to anaphase onset until 20 minutes post-anaphase onset. Spindle length at anaphase onset was determined for a given cell by selecting the spindle length at the time point prior to which an increase in spindle length of at least 0.2 microns was observed and followed by an increase in spindle length over the next 3 time points. Maximum rate of spindle elongation for a given cell was calculated by determining

the maximum difference in spindle length over a 2-minute time period and calculating the rate of spindle elongation over that time period.

Immunoprecipitations

An α-Flag immunoprecipitation of Kap60-3Flag was performed (essentially as described in (Akiyoshi et al., 2010)) to purify Kap60 and associated binding partners from asynchronously growing *S. cerevisiae* cells as described below. Strains expressing *stu2-AID* were grown overnight in yeast peptone dextrose rich (YPD) medium and back diluted to OD_{600}≈0.4 in the morning. 30 minutes prior to harvest, once cells reached OD_{600}≈2-3, 500 µM auxin was added to the culture to degrade Stu2-AID. Protein lysates were prepared by lysing cells in a Freezer/Mill submerged in liquid nitrogen. Lysed cells were resuspended in buffer H (BH) (25 mM HEPES pH 8.0, 2 mM $MgCl_2$, 0.1 mM EDTA, 0.5 mM EGTA, 0.1% NP-40, 15% glycerol with 150 mM KCl) containing protease inhibitors (at 20 µg mL^{-1} final concentration for each of leupeptin, pepstatin A, chymostatin and 200 µM phenylmethylsulfonyl fluoride) and phosphatase inhibitors (0.1 mM Na-orthovanadate, 0.2 µM microcystin, 2 mM β-glycerophosphate, 1 mM Na pyrophosphate, 5 mM NaF) followed by ultracentrifugation at 98,500 g for 90 min at 4°C. Dynabeads conjugated with α-Flag were incubated with extract for 3 h with constant rotation, followed by three washes with BH containing protease inhibitors, phosphatase inhibitors, 2 mM dithiothreitol (DTT) and 150 mM KCl. Beads were further washed twice with BH containing 150 mM KCl and protease inhibitors. Associated proteins were eluted from the beads by incubation in 1x SDS sample buffer at 95°C for 3 min.

Immunoblotting

For immunoblot analysis, cell lysates were prepared as described above. Standard procedures for sodium dodecyl sulfate-polyacrylamide gel electrophoresis (SDS-PAGE) and immunoblotting were followed as described in (Burnette, 1981; Towbin et al., 1992). A nitrocellulose membrane (Bio-Rad) was used to transfer proteins from polyacrylamide gels. Commercial antibodies used for immunoblotting were as follows: α-Flag, M2 (Sigma-Aldrich) 1:3,000; α-V5 (Invitrogen) 1:5,000; Pgk1 (Abcam) 1:5,000. The secondary antibodies used were a sheep anti-mouse antibody conjugated to horseradish peroxidase (HRP) (GE Biosciences) at a 1:10,000 dilution. Antibodies were detected using the SuperSignal West Dura Chemiluminescent Substrate (Thermo Scientific) and ProSignal Femto substrate (Genesee Scientific).

Statistics

GraphPad Prism version 9.1 was used for statistical analysis. Data normality was assumed for all experiments. Student's *t* test was used for comparisons between groups. In the text, mean ± SEM is reported.

Multiple sequence alignments

Fungal proteins related to *Saccharomyces cerevisiae* Stu2 were identified using a PSI-BLAST (Altschul et al., 1997) search on NCBI. Multiple sequence alignments of the entire proteins were generated with ClustalOmega default parameters and displayed in JalView 1.8.

Whole cell lysate polymerase assay

All strains were grown in standard rich media (YPD) at 25°C since they contained a temperature-sensitive allele. Cells were harvested as previously described in (Bergman et al., 2019). In short, strains were grown overnight and then diluted back into two identical 2L cultures of YPD with 2% glucose. At an OD_{600}≈0.4 cultures were then shifted to the non-permissive temperature of 29°C for a 3-hour arrest. Strains with AID degrons were treated with 250 µM auxin (3-indole acetic acid; Sigma-Alrich) in DMSO 30 minutes before harvesting, 2.5 hours into the arrest. Cells were then harvested by serial centrifugation at 6000 rpm in a Sorvall RC5B with a SLA-3000 rotor for 10 minutes at 4°C. Cell pellets were then resuspended in cold ddH_2O and pelleted in a Hermle Z446K centrifuge for 3 mins at 4000 rpm 4°C. This was repeated twice more, with the last spin (omitting the wash) to remove all standing water from the pellet via aspiration. The cells were then snap-frozen in liquid nitrogen and stored at -80°C.

As previous described, approximately 5g of frozen cell pellet was weighed out into a pre-chilled medium-sized SPEX freezer mill vial. The pre-chilled chamber was then milled (submerged in liquid nitrogen) following a protocol that consisted of a 3 minute pre-chill, then 10 cycles of 3 minutes grinding at 30 impacts per second (15 cps) and 1 minute of rest. The resulting powered lysate was stored at -80°C.

As previously described in (Bergman et al., 2019), previously purified bovine tubulin was cycled to remove nonfunctional tubulin and any remaining impurities. This tubulin was mixed with both biotin-conjugated and rhodamine labeled porcine tubulin (Cytoskeleton Inc.). The tubulin mix was then resuspended in PEM buffer (80 mM PIPES pH 6.9, 1 mM EGTA, 1 mM MgCl2) to a final concentration of 5 mg/mL unlabeled tubulin, 1 mg/mL biotin-labeled tubulin, and 1 mg/mL far-red labeled tubulin. To stabilize the seeds, GMPCPP (Jena Bioscienes) was added to a final concentration of 1 mM. Aliquots were then snap-frozen in liquid nitrogen and stored at -80°C.

Both glass side preparation and passivation of coverslips was similar to the protocol previously described in (Bergman et al., 2019). To prepare the glass sides for assembly into a flow chamber, microscope slides (Corning Inc.) were washed in acetone for 15 minutes and then 100% ethanol for 15 minutes. These slides were left to air dry before being stored in an airtight container.

To prepare the coverslips for assembly into a flow chamber, cover glass (1.5 thickness, Corning Inc.) was first cleaned by sonication in acetone for 30 minutes. The coverslips were then soaked for 15 minutes in 100% ethanol. After 3 thorough, but short, rinses in ddH_2O, the coverslips were submerged for 2 hours in 2% Hellmanex III solution (Hellma Analytics). After this, they were again rinsed in ddH_2O 3 times. Before proceeding to passivation, the coverslips were blown dry with nitrogen gas. For passivation, a solution containing 0.1 mg/mL pLL-g-PEG:PEG(3.4)-biotin (50%:50%) (SuSoS AG) in 10 mM HEPES was prepared. 50 uL drops were then placed on Parafilm in a humid chamber and coverslips were gently placed onto the

drops. After 1 hour, the passivated coverslips were washed for 2 minutes in PBS and rinsed in ddH_2O for 1 minute. Again, the coverslips were blown dry with nitrogen gas and stored in an airtight container at 4°C. These passivated coverslips were used for up to 3 weeks, maximum.

Preparation and assembly of the flow chamber for use in the TIRF based dynamics assay was exactly the same as described in (Bergman et al., 2019).

Similar to (Bergman et al., 2019), 0.22 g of powdered lysate was weighed out into a 1.5 mL eppendorf tube pre-chilled in liquid nitrogen. To the powder, 12.5 µL of cold 10X PEM (800 mM PIPES pH 6.9, 10 mM MgCl2, 10 mM EGTA), 0.5 µL of Protease Inhibitor Cocktail IV (Calbiochem), and 2.5 µL of 10 µM Halo conjugated JF646 dye in DMSO was added, spun down briefly, and let to sit on ice for 10 minutes. Lysate was added to pre-chilled polycarbonate ultracentrifuge tubes and cleared of insoluble material by spinning at 34,600 ***g*** for 25 minutes at 4°C. After ultracentrifugation, 32 µL of cleared soluble lysate was flowed into the chamber prepared previously (see above).

After clarified soluble lysate was added to the prepared chamber, the slides were loaded onto a Nikon Ti2-E inverted microscope with an Oko Labs environmental chamber pre-warmed to 28°C. Images were acquired with a Nikon 60X CFI Apo TIRF objective (NA 1.49) and an Orca Fusion Gen III sCMOS camera (Hamamatsu) at 1.5X magnification using the Nikon NIS Elements software. Using a LUNF 4-line laser launch (Nikon) and an iLas2 TIRF/FRAP module (Gataca Systems) total internal reflection fluorescence illuminated a single focal plane of the field and was imaged every 5 seconds for 30 minutes.

Analysis was done as described previously in (Bergman et al., 2019). Imaging data was analyzed using (Fiji is Just) ImageJ (NIH). Registration to correct for stage drift was applied to the raw data (Preibisch et al., 2010; Thévenaz et al., 1998). Kymographs were generated from all microtubules whose entire length was trackable for the entire movie. Kymographs were excluded if the microtubules were crossed or were bundled. For analysis, data from independent technical trials and biological replicas from one genotype were pooled, unless otherwise indicated.

Protein expression and purification

αβ-tubulin from yeast was overexpressed in *S. cerevisiae* and purified using Ni-affinity and ion exchange chromatography, as previously described in (Geyer et al., 2015) but with minor modifications. $Stu2^{KR/AA}$ mutations were introduced into the $Stu2^{WT}$ background using QuikChange (Stratagene) mutagenesis. All Stu2 constructs were expressed in *E. coli* using Arctic Express Cells, and were induced with 0.5 mM IPTG at 10°C for 24 hrs. Cell pellets were resuspended in lysis buffer (50 mM sodium phosphate dibasic and monobasic mix, 300 mM NaCl, 40 mM imidazole, 5% glycerol), PMSF was added to 1 mM final concentration, and lysed using a microfluidizer. The lysate was then clarified by centrifugation before loading onto a His60 Superflow Column (Clontech) and eluted in lysis buffer containing 300 mM imidazole. Pooled elution fractions were then loaded onto a Strep-Tactin Superflow column (IBA,

Germany) and eluted in RB100 (25 mM Tris pH 7.5, 100 mM NaCl, 1 mM $MgCl_2$, 1 mM EGTA) containing 10 mM desthiobiotin. For storage, eluted samples were exchanged into RB100 with 2 mL, 7K MWCO Zeba spin desalting columns (Thermo Scientific).

In vitro microtubule dynamics assay

Assay chambers were assembled from slides, cover slips, and double sticky tape as previously described (Geyer et al., 2015). Chambers were preincubated with neutravidin (5 µg/ml) and blocked with 1% F-127 Pluronic acid for 10 and 5 mins respectively. The chambers were then rinsed with BRB80 (80 mM PIPES pH 6.9, 1 mM $MgCl_2$, 1 mM EGTA) followed by 10 min incubation with GMPCPP seeds made from brain tubulin (5% biotinylated, PurSolutions). Chambers were rinsed again with BRB80 and samples containing αβ-tubulin and accessory protein ($Stu2^{WT}$ or $Stu2^{KR/AA}$) in 1× PEM + 0.1 mg/ml bovine serum albumin (BSA) + 1 mM GTP were flowed into the same and immediately sealed with VALAP. Microtubule dynamics were measured by time-lapse DIC microscopy, as described previously in (Geyer et al., 2015).

Online Supplemental material

Fig. S1 shows conservation of the entire basic linker region of Stu2 across 9 fungal species as well as viability assays of various mutants within $Stu2^{592-606}$, related to Fig. 1. Fig. S2 shows further characterization of basic linker mutants' ability to form a mitotic spindle and regulate microtubule dynamics, related to Fig. 2. Fig. S3 shows the ratio of nuclear to cytoplasmic GFP signal intensity in $Stu2^{592-607}$-GFP-GST with a copy of GFP that is unable to dimerize, related to Fig. 3. Fig. S4 examines cell cycle dependent regulation of nuclear import of $Stu2^{592-607}$-GFP-GST and specifically the effects of phosphorylation deficient and phosphorylation mimicking mutations of $Stu2^{S603}$, as related to Fig. 4. Fig. S5 shows a viability assay of strains expressing alleles containing *stu2*$^{KR/AA}$ in combination with phosphorylation deficient and phosphorylation mimicking NES regulatory elements, and representative kymographs related to Fig. 5.

REFERENCES

Akiyoshi, B., Sarangapani, K. K., Powers, A. F., Nelson, C. R., Reichow, S. L., Arellano-Santoyo, H., Gonen, T., Ranish, J. A., Asbury, C. L., & Biggins, S. (2010). Tension directly stabilizes reconstituted kinetochore-microtubule attachments. *Nature*, *468*(7323), 576–579. https://doi.org/10.1038/nature09594

Al-Bassam, J., & Chang, F. (2011). Regulation of microtubule dynamics by TOG-domain proteins XMAP215/Dis1 and CLASP. *Trends in Cell Biology*, *21*(10), 604–614. https://doi.org/10.1016/j.tcb.2011.06.007

Al-Bassam, J., van Breugel, M., Harrison, S. C., & Hyman, A. (2006). Stu2p binds tubulin and undergoes an open-to-closed conformational change. *The Journal of Cell Biology*, *172*(7), 1009–1022. https://doi.org/10.1083/jcb.200511010

Albuquerque, C. P., Smolka, M. B., Payne, S. H., Bafna, V., Eng, J., & Zhou, H. (2008). A Multidimensional Chromatography Technology for In-depth Phosphoproteome Analysis. *Molecular & Cellular Proteomics : MCP*, *7*(7), 1389–1396. https://doi.org/10.1074/mcp.M700468-MCP200

Altschul, S. F., Madden, T. L., Schäffer, A. A., Zhang, J., Zhang, Z., Miller, W., & Lipman, D. J. (1997). Gapped BLAST and PSI-BLAST: A new generation of protein database search programs. *Nucleic Acids Research*, *25*(17), 3389–3402. https://doi.org/10.1093/nar/25.17.3389

Ayaz, P., Munyoki, S., Geyer, E. A., Piedra, F.-A., Vu, E. S., Bromberg, R., Otwinowski, Z., Grishin, N. V., Brautigam, C. A., & Rice, L. M. (2014). A tethered delivery mechanism explains the catalytic action of a microtubule polymerase. *ELife*, *3*, e03069. https://doi.org/10.7554/eLife.03069

Bergman, Z. J., Wong, J., Drubin, D. G., & Barnes, G. (2019). Microtubule dynamics regulation reconstituted in budding yeast lysates. *Journal of Cell Science*, *132*(4), jcs219386. https://doi.org/10.1242/jcs.219386

Bodakuntla, S., Jijumon, A. S., Villablanca, C., Gonzalez-Billault, C., & Janke, C. (2019). Microtubule-Associated Proteins: Structuring the Cytoskeleton. *Trends in Cell Biology*, *29*(10), 804–819. https://doi.org/10.1016/j.tcb.2019.07.004

Brouhard, G. J., Stear, J. H., Noetzel, T. L., Al-Bassam, J., Kinoshita, K., Harrison, S. C., Howard, J., & Hyman, A. A. (2008). XMAP215 is a processive microtubule polymerase. *Cell*, *132*(1), 79–88. https://doi.org/10.1016/j.cell.2007.11.043

Burnette, W. N. (1981). “Western blotting”: Electrophoretic transfer of proteins from sodium dodecyl sulfate—Polyacrylamide gels to unmodified nitrocellulose and radiographic detection with antibody and radioiodinated protein A. *Analytical Biochemistry*, *112*(2), 195–203.

Caudron, M., Bunt, G., Bastiaens, P., & Karsenti, E. (2005). Spatial Coordination of Spindle Assembly by Chromosome-Mediated Signaling Gradients. *Science*, *309*(5739), 1373–1376. https://doi.org/10.1126/science.1115964

Chen, X. P., Yin, H., & Huffaker, T. C. (1998). The Yeast Spindle Pole Body Component Spc72p Interacts with Stu2p and Is Required for Proper Microtubule Assembly. *Journal of Cell Biology*, *141*(5), 1169–1179. https://doi.org/10.1083/jcb.141.5.1169

Christie, M., Chang, C.-W., Róna, G., Smith, K. M., Stewart, A. G., Takeda, A. A. S., Fontes, M. R. M., Stewart, M., Vértessy, B. G., Forwood, J. K., & Kobe, B. (2016). Structural Biology and Regulation of Protein Import into the Nucleus. *Journal of Molecular Biology*, *428*(10, Part A), 2060–2090. https://doi.org/10.1016/j.jmb.2015.10.023

Clarke, P. R., & Zhang, C. (2008). Spatial and temporal coordination of mitosis by Ran GTPase. *Nature Reviews. Molecular Cell Biology*, *9*(6), 464–477. https://doi.org/10.1038/nrm2410

Dasso, M. (2001). Running on Ran: Nuclear Transport and the Mitotic Spindle. *Cell*, *104*(3), 321–324. https://doi.org/10.1016/S0092-8674(01)00218-5

Enenkel, C., Blobel, G., & Rexach, M. (1995). Identification of a yeast karyopherin heterodimer that targets import substrate to mammalian nuclear pore complexes. *The Journal of Biological Chemistry*, *270*(28), 16499–16502. https://doi.org/10.1074/jbc.270.28.16499

Faustova, I., Örd, M., Kiselev, V., Fedorenko, D., Borovko, I., Macs, D., Pääbo, K., Lõoke, M., & Loog, M. (2022). A synthetic biology approach reveals diverse and dynamic CDK response profiles via multisite phosphorylation of NLS-NES modules. *Science Advances*, *8*(33), eabp8992. https://doi.org/10.1126/sciadv.abp8992

Fees, C. P., Estrem, C., & Moore, J. K. (2017). High-resolution Imaging and Analysis of Individual Astral Microtubule Dynamics in Budding Yeast. *Journal of Visualized Experiments : JoVE*, *122*, 55610. https://doi.org/10.3791/55610

Geyer, E. A., Burns, A., Lalonde, B. A., Ye, X., Piedra, F.-A., Huffaker, T. C., & Rice, L. M. (2015). A mutation uncouples the tubulin conformational and GTPase cycles, revealing allosteric control of microtubule dynamics. *ELife*, *4*, e10113. https://doi.org/10.7554/eLife.10113

Geyer, E. A., Miller, M. P., Brautigam, C. A., Biggins, S., & Rice, L. M. (2018). Design principles of a microtubule polymerase. *ELife*, *7*, e34574. https://doi.org/10.7554/eLife.34574

Gudimchuk, N. B., & McIntosh, J. R. (2021). Regulation of microtubule dynamics, mechanics and function through the growing tip. *Nature Reviews Molecular Cell Biology*, *22*(12), 777–795. https://doi.org/10.1038/s41580-021-00399-x

Gunzelmann, J., Rüthnick, D., Lin, T.-C., Zhang, W., Neuner, A., Jäkle, U., & Schiebel, E. (2018). The microtubule polymerase Stu2 promotes oligomerization of the γ-TuSC for cytoplasmic microtubule nucleation. *ELife*, *7*. https://doi.org/10.7554/eLife.39932

Hagan, I. M., & Hyams, J. S. (1988). The use of cell division cycle mutants to investigate the control of microtubule distribution in the fission yeast Schizosaccharomyces pombe. *Journal of Cell Science*, *89 (Pt 3)*, 343–357.

Hayles, J., Fisher, D., Woollard, A., & Nurse, P. (1994). Temporal order of S phase and mitosis in fission yeast is determined by the state of the p34cdc2-mitotic B cyclin complex. *Cell*, *78*(5), 813–822. https://doi.org/10.1016/s0092-8674(94)90542-8

Herman, J. A., Miller, M. P., & Biggins, S. (2020). ChTOG is a conserved mitotic error correction factor. *ELife*, *9*, e61773. https://doi.org/10.7554/eLife.61773

Holt, L. J., Tuch, B. B., Villén, J., Johnson, A. D., Gygi, S. P., & Morgan, D. O. (2009). Global analysis of Cdk1 substrate phosphorylation sites provides insights into evolution. *Science (New York, N.Y.)*, *325*(5948), 1682. https://doi.org/10.1126/science.1172867

Humphrey, L., Felzer-Kim, I., & Joglekar, A. P. (2018). Stu2 acts as a microtubule destabilizer in metaphase budding yeast spindles. *Molecular Biology of the Cell*, *29*(3), 247–255. https://doi.org/10.1091/mbc.E17-08-0494

Jans, D. A., Xiao, C. Y., & Lam, M. H. (2000). Nuclear targeting signal recognition: A key control point in nuclear transport? *BioEssays: News and Reviews in Molecular, Cellular and Developmental Biology*, *22*(6), 532–544. https://doi.org/10.1002/(SICI)1521-1878(200006)22:6<532::AID-BIES6>3.0.CO;2-O

Kalab, P., & Heald, R. (2008). The RanGTP gradient – a GPS for the mitotic spindle. *Journal of Cell Science*, *121*(10), 1577–1586. https://doi.org/10.1242/jcs.005959

Kaláb, P., Pralle, A., Isacoff, E. Y., Heald, R., & Weis, K. (2006). Analysis of a RanGTP-regulated gradient in mitotic somatic cells. *Nature*, *440*(7084), 697–701. https://doi.org/10.1038/nature04589

Kalab, P., Weis, K., & Heald, R. (2002). Visualization of a Ran-GTP Gradient in Interphase and Mitotic Xenopus Egg Extracts. *Science*, *295*(5564), 2452–2456. https://doi.org/10.1126/science.1068798

King, B. R., Meehl, J. B., Vojnar, T., Winey, M., Muller, E. G., & Davis, T. N. (2021). Microtubule-associated proteins and motors required for ectopic microtubule array formation in Saccharomyces cerevisiae. *Genetics*, *218*(2), iyab050. https://doi.org/10.1093/genetics/iyab050

King, B. R., Moritz, M., Kim, H., Agard, D. A., Asbury, C. L., & Davis, T. N. (2020). XMAP215 and γ-tubulin additively promote microtubule nucleation in purified solutions. *Molecular Biology of the Cell*, *31*(20), 2187–2194. https://doi.org/10.1091/mbc.E20-02-0160

Kinoshita, K., Habermann, B., & Hyman, A. A. (2002). XMAP215: A key component of the dynamic microtubule cytoskeleton. *Trends in Cell Biology*, *12*(6), 267–273. https://doi.org/10.1016/S0962-8924(02)02295-X

Kirschner, M., & Mitchison, T. (1986). Beyond self-assembly: From microtubules to morphogenesis. *Cell*, *45*(3), 329–342. https://doi.org/10.1016/0092-8674(86)90318-1

Kosco, K. A., Pearson, C. G., Maddox, P. S., Wang, P. J., Adams, I. R., Salmon, E. D., Bloom, K., & Huffaker, T. C. (2001). Control of microtubule dynamics by Stu2p is essential for spindle orientation and metaphase chromosome alignment in yeast. *Molecular Biology of the Cell*, *12*(9), 2870–2880.

Kosugi, S., Hasebe, M., Matsumura, N., Takashima, H., Miyamoto-Sato, E., Tomita, M., & Yanagawa, H. (2009). Six Classes of Nuclear Localization Signals Specific to Different Binding Grooves of Importin α*. *Journal of Biological Chemistry*, *284*(1), 478–485. https://doi.org/10.1074/jbc.M807017200

Lanz, M. C., Yugandhar, K., Gupta, S., Sanford, E. J., Faça, V. M., Vega, S., Joiner, A. M. N., Fromme, J. C., Yu, H., & Smolka, M. B. (2021). In-depth and 3-dimensional exploration of the budding yeast phosphoproteome. *EMBO Reports*, *22*(2), e51121. https://doi.org/10.15252/embr.202051121

Liu, H., & Naismith, J. H. (2008). An efficient one-step site-directed deletion, insertion, single and multiple-site plasmid mutagenesis protocol. *BMC Biotechnology*, *8*(1), 91. https://doi.org/10.1186/1472-6750-8-91

Longtine, M. S., McKenzie, A., Demarini, D. J., Shah, N. G., Wach, A., Brachat, A., Philippsen, P., & Pringle, J. R. (1998). Additional modules for versatile and economical PCR-based gene deletion and modification in Saccharomyces cerevisiae. *Yeast*, *14*(10), 953–961. https://doi.org/10.1002/(SICI)1097-0061(199807)14:10<953::AID-YEA293>3.0.CO;2-U

MacGilvray, M. E., Shishkova, E., Place, M., Wagner, E. R., Coon, J. J., & Gasch, A. P. (2020). The phosphoproteome response to dithiothreitol reveals unique versus shared features of Saccharomyces cerevisiae stress responses. *Journal of Proteome Research*, *19*(8), 3405–3417. https://doi.org/10.1021/acs.jproteome.0c00253

Miller, M. P., Asbury, C. L., & Biggins, S. (2016). A TOG Protein Confers Tension Sensitivity to Kinetochore-Microtubule Attachments. *Cell*, *165*(6), 1428–1439. https://doi.org/10.1016/j.cell.2016.04.030

Miller, M. P., Evans, R. K., Zelter, A., Geyer, E. A., MacCoss, M. J., Rice, L. M., Davis, T. N., Asbury, C. L., & Biggins, S. (2019). Kinetochore-associated Stu2 promotes chromosome biorientation in vivo. *PLoS Genetics*, *15*(10), e1008423. https://doi.org/10.1371/journal.pgen.1008423

Nardozzi, J. D., Lott, K., & Cingolani, G. (2010). Phosphorylation meets nuclear import: A review. *Cell Communication and Signaling : CCS*, *8*, 32. https://doi.org/10.1186/1478-811X-8-32

Nishimura, K., Fukagawa, T., Takisawa, H., Kakimoto, T., & Kanemaki, M. (2009). An auxin-based degron system for the rapid depletion of proteins in nonplant cells. *Nature Methods*, *6*(12), 917–922. https://doi.org/10.1038/nmeth.1401

Nithianantham, S., Cook, B. D., Beans, M., Guo, F., Chang, F., & Al-Bassam, J. (2018). Structural basis of tubulin recruitment and assembly by microtubule polymerases with tumor overexpressed gene (TOG) domain arrays. *ELife*, *7*, e38922. https://doi.org/10.7554/eLife.38922

Ohkura, H., Garcia, M. A., & Toda, T. (2001). Dis1/TOG universal microtubule adaptors—One MAP for all? *Journal of Cell Science*, *114*(21), 3805–3812. https://doi.org/10.1242/jcs.114.21.3805

Okada, N., Toda, T., Yamamoto, M., & Sato, M. (2014). CDK-dependent phosphorylation of Alp7-Alp14 (TACC-TOG) promotes its nuclear accumulation and spindle microtubule assembly. *Molecular Biology of the Cell*, *25*(13), 1969–1982. https://doi.org/10.1091/mbc.E13-11-0679

Pearson, C. G., Maddox, P. S., Zarzar, T. R., Salmon, E. D., & Bloom, K. (2003). Yeast kinetochores do not stabilize Stu2p-dependent spindle microtubule dynamics. *Molecular Biology of the Cell*, *14*(10), 4181–4195. https://doi.org/10.1091/mbc.E03-03-0180

Podolski, M., Mahamdeh, M., & Howard, J. (2014). Stu2, the budding yeast XMAP215/Dis1 homolog, promotes assembly of yeast microtubules by increasing growth rate and decreasing catastrophe frequency. *The Journal of Biological Chemistry*, *289*(41), 28087–28093. https://doi.org/10.1074/jbc.M114.584300

Preibisch, S., Saalfeld, S., Schindelin, J., & Tomancak, P. (2010). Software for bead-based registration of selective plane illumination microscopy data. *Nature Methods*, *7*(6), 418–419. https://doi.org/10.1038/nmeth0610-418

Roostalu, J., Cade, N. I., & Surrey, T. (2015). Complementary activities of TPX2 and chTOG constitute an efficient importin-regulated microtubule nucleation module. *Nature Cell Biology*, *17*(11), 1422–1434. https://doi.org/10.1038/ncb3241

Severin, F., Habermann, B., Huffaker, T., & Hyman, T. (2001). Stu2 promotes mitotic spindle elongation in anaphase. *The Journal of Cell Biology*, *153*(2), 435–442.

Sherman, F., Fink, G., & Lawrence, C. (1974). *Methods in Yeast Genetics*. Cold Spring Harbor, New York: Cold Spring Harbor Laboratory Press.

Shrestha, S., Ems-McClung, S. C., Hazelbaker, M. A., Yount, A. L., Shaw, S. L., & Walczak, C. E. (2022). *Emerging Roles of Importin α/β and EB1 in Differential Regulation of Kif18B Astral Microtubule Destabilization* (p. 2022.03.30.486445). bioRxiv. https://doi.org/10.1101/2022.03.30.486445

Swaney, D. L., Beltrao, P., Starita, L., Guo, A., Rush, J., Fields, S., Krogan, N. J., & Villén, J. (2013). Global analysis of phosphorylation and ubiquitylation crosstalk in protein degradation. *Nature Methods*, *10*(7), 10.1038/nmeth.2519. https://doi.org/10.1038/nmeth.2519

Thévenaz, P., Ruttimann, U. E., & Unser, M. (1998). A pyramid approach to subpixel registration based on intensity. *IEEE Transactions on Image Processing*, *7*(1), 27–41. https://doi.org/10.1109/83.650848

Towbin, H., Staehelin, T., & Gordon, J. (1992). Electrophoretic transfer of proteins from polyacrylamide gels to nitrocellulose sheets: Procedure and some applications. 1979. *Biotechnology (Reading, Mass.)*, *24*, 145–149.

Tran, P. T., Marsh, L., Doye, V., Inoué, S., & Chang, F. (2001). A mechanism for nuclear positioning in fission yeast based on microtubule pushing. *The Journal of Cell Biology*, *153*(2), 397–411. https://doi.org/10.1083/jcb.153.2.397

Tseng, W.-C., Lin, J.-W., Wei, T.-Y., & Fang, T.-Y. (2008). A novel megaprimed and ligase-free, PCR-based, site-directed mutagenesis method. *Analytical Biochemistry*, *375*(2), 376–378. https://doi.org/10.1016/j.ab.2007.12.013

Usui, T., Maekawa, H., Pereira, G., & Schiebel, E. (2003). The XMAP215 homologue Stu2 at yeast spindle pole bodies regulates microtubule dynamics and anchorage. *The EMBO Journal*, *22*(18), 4779–4793. https://doi.org/10.1093/emboj/cdg459

van Breugel, M., Drechsel, D., & Hyman, A. (2003). Stu2p, the budding yeast member of the conserved Dis1/XMAP215 family of microtubule-associated proteins is a plus end-binding microtubule destabilizer. *The Journal of Cell Biology*, *161*(2), 359–369. https://doi.org/10.1083/jcb.200211097

van der Vaart, B., Fischböck, J., Mieck, C., Pichler, P., Mechtler, K., Medema, R. H., & Westermann, S. (2017). TORC1 signaling exerts spatial control over microtubule dynamics by promoting nuclear export of Stu2. *The Journal of Cell Biology*, *216*(11), 3471–3484. https://doi.org/10.1083/jcb.201606080

Wang, P. J., & Huffaker, T. C. (1997). Stu2p: A microtubule-binding protein that is an essential component of the yeast spindle pole body. *The Journal of Cell Biology*, *139*(5), 1271–1280.

Widlund, P. O., Stear, J. H., Pozniakovsky, A., Zanic, M., Reber, S., Brouhard, G. J., Hyman, A. A., & Howard, J. (2011). XMAP215 polymerase activity is built by combining multiple tubulin-binding TOG domains and a basic lattice-binding region.

Proceedings of the National Academy of Sciences of the United States of America, *108*(7), 2741–2746. https://doi.org/10.1073/pnas.1016498108

Wolyniak, M. J., Blake-Hodek, K., Kosco, K., Hwang, E., You, L., & Huffaker, T. C. (2006). The Regulation of Microtubule Dynamics in Saccharomyces cerevisiae by Three Interacting Plus-End Tracking Proteins. *Molecular Biology of the Cell*, *17*(6), 2789–2798. https://doi.org/10.1091/mbc.E05-09-0892

Zacharias, D. A., Violin, J. D., Newton, A. C., & Tsien, R. Y. (2002). Partitioning of Lipid-Modified Monomeric GFPs into Membrane Microdomains of Live Cells. *Science*. https://doi.org/10.1126/science.1068539

Zahm, J. A., Stewart, M. G., Carrier, J. S., Harrison, S. C., & Miller, M. P. (2021). Structural basis of Stu2 recruitment to yeast kinetochores. *ELife*, *10*, e65389. https://doi.org/10.7554/eLife.65389

FIGURE LEGENDS

Figure 1. Two positive residues within a conserved patch in Stu2's basic linker region are essential for cell viability.

(A) Schematic of Stu2's domains (NES, nuclear export sequence; CTS, c-terminal segment).

(B) Multiple sequence alignment across 9 different fungal species reveals a conserved patch of amino acids within Stu2's basic linker region.

(C) Cell viability was analyzed in *stu2-AID* strains without a covering allele (M619) or ectopically expressing Stu2 (*STU2*^{WT}, M622; *stu2*^{P596A}, M1290; *stu2*^{S597A}, M1299; *stu2*^{K598A}, M954; *stu2*^{R599A}, M956; *stu2*$^{V600A\ S602A}$, M1383; or *stu2*^{S603A}, M802) by plating five-fold serial dilutions in the presence of DMSO (left) or auxin (right) to degrade the endogenous Stu2-AID protein.

(D) Exponentially growing *stu2-AID* strains without a covering allele (M619) or ectopically expressing *STU2-3V5* alleles (*STU2*^{WT}, M622; *stu2*^{P596A}, M1290; *stu2*^{S597A}, M1299; *stu2*^{K598A}, M954; *stu2*^{R599A}, M956; *stu2*$^{V600A\ S602A}$, M1383; *stu2*^{S603A}, M802; or *stu2*$^{K598A\ R599A}$, M888) were treated with auxin 30 min prior to harvesting. Protein lysates were subsequently prepared and expression of Stu2-3V5 proteins were analyzed by immunoblotting. Pgk1 is shown as a loading control.

Figure 2. Cells expressing *stu2*$^{KR/AA}$ have pleiotropic mitotic defects despite normal microtubule regulatory activity.

(A) Schematic of the *stu2* constructs in Fig. 2 B,C.

(B) Exponentially growing *stu2-AID cdc20-AID* cells ectopically expressing Stu2 (*STU2*^{WT}, M1914; *stu2*$^{\Delta BL}$, M1918; *stu2*$^{\Delta 592-606}$, M1921; or *stu2*$^{KR/AA}$, M1922) were treated with auxin for 2 hours to degrade Stu2-AID and Cdc20-AID, arresting cells in metaphase. Cells were fixed and the Spc110-mCherry signal was imaged. In cells with bipolar mCherry punctae, the distance was measured between these punctae, and is indicated by a data point for each cell. Median and the 95% confidence interval are shown. n = 90–116 cells; p values were determined using a two-tailed unpaired t test (*** = $p<0.0001$).

(C) Exponentially growing *GFP-TUB1 stu2-AID cdc23-1* cells with no covering allele (M2166) or ectopically expressing Stu2-Halo (*STU2*^{WT}, M2231; *stu2*$^{\Delta BL}$, M2360; *stu2*$^{\Delta 592-606}$, M2234; or *stu2*$^{KR/AA}$, M2232) were shifted to a non-permissive temperature for 3 hours to arrest cells in metaphase and treated with auxin for 30 minutes to degrade Stu2-AID. Whole cell lysate was incubated with microtubule seeds, and growth and shrinkage rates of microtubule extensions were determined. Top: Representative kymograph of *STU2*^{WT} (red, microtubule extension; cyan, seed). Rates of microtubule assembly or disassembly are determined by the slope of microtubule extension growth and shrinkage over time. Bottom left: Assembly rates of microtubules. Each data point represents an independent microtubule assembly event. Median and the 95% confidence interval are shown. n=105-322 growth events. Right: Disassembly rates of microtubules. Each data point represents an independent microtubule disassembly event. Median and the 95% confidence interval are shown. n=19-190 shrinkage events; p values were determined using a two-tailed unpaired t test (*** = $p<0.0001$).

(D) Top: representative kymograph (+Stu2^{WT}). Bottom: Quantification of MT growth rates with yeast αβ-tubulin (0.8 μM) without Stu2 or with 250 nM Stu2^{WT} or Stu2$^{KR/AA}$, as indicated. Average growth rates for αβ-tubulin, αβ-tubulin+Stu2^{WT} and αβ-tubulin+Stu2$^{KR/AA}$ were 0.267 ± 0.045 μm/min (n=26), 2.269 ± 0.333 μm/min (n= 28), and 1.879 ± 0.493 μm/min (n=23), respectively.

(E) Exponentially growing *stu2-AID cdc20-AID* cells ectopically expressing Stu2 (*STU2^{WT}*, M1914; or *stu2$^{KR/AA}$*, M1922) were treated with auxin for 2 hours. Cells were fixed and both the Spc110-mCherry signal and Mtw1-GFP signal were imaged. Left: Cells with a mono-lobed GFP puncta versus bi-lobed GFP punctae were counted. Proportion of cells for each strain with a mono-lobed GFP puncta are shown, n=101-103 cells (top). Representative images of cells with a mono-lobed versus bi-lobed GFP puncta (bottom). Middle: Cells with a mitotic spindle oriented within 45 degrees of the mother-daughter bud axis versus greater than 45 degrees were counted. Proportion of cells with a spindle oriented greater than 45 degrees relative to the mother-daughter bud axis (top). Representative cells with an oriented versus misoriented spindle (bottom). Right: Cells with a GFP puncta isolated from the normal bipolar GFP punctae were counted and percentage of cells with an isolated puncta for each strain are shown, n=101-103 cells (top). Representative cells with and without an isolated GFP puncta (bottom).

Figure 3. Stu2$^{592-607}$ is required to import Stu2 into the nucleus.

(A) Exponentially growing *NUP2-mKATE stu2-AID cdc20-AID* cells ectopically expressing *STU2-GFP* alleles (*STU2^{WT}*, M2208; or *stu2$^{KR/AA}$*, M2210) were treated with auxin for 2 hours. Cells were fixed and imaged for DAPI, Nup2-mKATE, and Stu2-GFP. Left: Representative images of DIC, DAPI, Nup2-mKATE, and Stu2^{WT}-GFP (top) or Stu2$^{KR/AA}$-GFP signals (bottom) with a representative outline of the nucleus. Right: Quantification of the ratio of the nuclear to cytoplasmic GFP signal intensities with each data point representing a measurement from a single cell. Median and the 95% confidence interval are shown. n=96-160 cells; p values were determined using a two-tailed unpaired t test (*** = $p<0.0001$).

(B) Exponentially growing *stu2-AID* cells expressing Kap60-3FLAG without a covering *STU2* allele (M2350) or ectopically expressing *STU2-3V5* alleles (*STU2^{WT}*, M2435; or *stu2$^{KR/AA}$*, M2436) were treated with auxin 30 min prior to harvesting. Protein lysates were subsequently prepared and Kap60 and associated binding partners were purified by α-Flag immunoprecipitation (IP) and associated Stu2-3V5 proteins were analyzed by immunoblotting.

(C) Exponentially growing *stu2-AID cdc20-AID* cells ectopically expressing GFP-GST fused constructs (GFP-GST, M2390; NLS^{SV40}-GFP-GST, M2391; Stu2$^{592-607}$-GFP-GST, M2392; or Stu2$^{592-607(KR/AA)}$-GFP-GST, M2437) were treated with auxin for 2 hours. Cells were fixed and the Nup2-mKATE and GFP signals were imaged. Left: Schematic of the constructs used. Middle: Representative images of DIC, Nup2-mKATE, and GFP signals for each strain with an outlined nucleus. Right: Quantification of the ratio of the nuclear to cytoplasmic GFP signal intensities. Each data point represents this ratio for a single cell. Median and the 95%

confidence interval are shown. n=111-161 cells; p values were determined using a two-tailed unpaired t test (*** = p<0.0001).

Figure 4. Stu2's nuclear localization is regulated by phosphorylation of Stu2^{S603}

(A) Exponentially growing *stu2-AID* cells ectopically expressing *STU2-GFP* alleles (*STU2^{WT}-GFP*, M2298; or *stu2^{S603A}-GFP*, M2351) were treated with α-factor for 2.5 hours to arrest cells in G1 then with auxin for 30 minutes to degrade Stu2-AID, or as above but with *cdc20-AID* (*STU2^{WT}-GFP*, M2208; or *stu2^{S603A}-GFP*, M2217) were treated with auxin for 2 hours to degrade Stu2-AID and Cdc20-AID to arrest cells in metaphase. Cells were fixed and Nup2-mKATE and Stu2-GFP signals were imaged. The ratios of nuclear to cytoplasmic GFP intensities were quantified. Each data point represents this ratio for a single cell. Median and the 95% confidence interval are shown. n=100-165 cells; p values were determined using a two-tailed unpaired t test (*** = p<0.0001).

(B) Proposed schematic of Stu2's nuclear import. Stu2$^{592-607}$ is required for binding to Kap60 to allow for Stu2 nuclear import. Mitosis specific phosphorylation of Stu2^{S603} by CDK promotes binding to Kap60 and nuclear import during mitosis.

Figure 5. Stu2's basic linker region is dispensable for cell viability outside of localizing Stu2 to the nucleus.

(A) Cell viability was analyzed in a wild-type strain (M3) and *stu2-AID* strains without a covering allele (M619) or ectopically expressing Stu2 alleles (*STU2^{WT}*, M2103; *STU2^{WT}-NLS^{SV40}*, M2105; *stu2$^{KR/AA}$*, M2225; or *stu2$^{KR/AA}$-NLS^{SV40}*, M2199) by plating five-fold serial dilutions in the presence of DMSO or auxin with or without 6.5 µg/mL benomyl.

(B) Exponentially growing *stu2-AID cdc20-AID* cells ectopically expressing *STU2-GFP* alleles (*STU2^{WT}*, M2208; *stu2$^{KR/AA}$*, M2210; or *stu2$^{KR/AA}$-NLS^{SV40}*, M2353) were treated with auxin for 2 hours. Cells were fixed and Stu2-GFP signals were imaged. The ratio of the nuclear to cytoplasmic GFP signal intensities was quantified. Each data point represents this ratio for a single cell. Median and the 95% confidence interval are shown. n=114-137 cells; p values were determined using a two-tailed unpaired t test (*** = p<0.0001).

(C) Left: Schematic of the *STU2* alleles used. Right: Cell viability was analyzed in *stu2-AID* strains ectopically expressing *STU2* alleles (*STU2^{WT}*, M2103; *stu2^{ΔBL}*, M2226; *stu2$^{ΔBL::592-606}$*, M2301; *STU2^{WT}-NLS^{SV40}*, M2105; *stu2^{ΔBL}-NLS^{SV40}*, M2107; *stu2$^{ΔBL::592-606}$-NLS^{SV40}*, M2302) by plating five-fold serial dilutions in the presence of DMSO, or auxin and DMSO, with or without 6.5 µg/mL benomyl.

(D) Exponentially growing *stu2-AID cdc20-AID* cells ectopically expressing Stu2 (*STU2^{WT}*, M1757; *stu2^{ΔBL}*, M1759; *STU2^{WT}-NLS^{SV40}*, M2125; or *stu2^{ΔBL}-NLS^{SV40}*, M2126) were treated with auxin for 2 hours. Cells were fixed and the Spc110-mCherry signal was imaged. Distance was measured between mCherry punctae in cells with a bipolar spindle. This distance for an individual cell is indicated by a data point. Median and the 95% confidence interval are shown. n = 90–116 cells; p values were determined using a two-tailed unpaired t test (*** = p<0.0001).

(E) Exponentially growing *stu2-AID* cells ectopically expressing Stu2-GFP (*STU2*^{WT}-*NLS*^{SV40}, M2729; *stu2*$^{\Delta BL}$-*NLS*^{SV40}, M2731) were treated with auxin for 30 minutes to degrade Stu2-AID. Spc110-mCherry and Stu2-GFP signals were imaged every minute. Representative time course of a cell progressing through anaphase beginning 5 minutes prior to anaphase onset until 20 minutes post-anaphase onset (merge of Spc110-mCherry and Stu2-GFP signals shown). The white dotted line indicates anaphase onset.

(F) Left: Average spindle length and 95% confidence intervals from 5 minutes prior to anaphase onset to 20 minutes post-anaphase onset. The black dotted line indicates anaphase onset. Lines with indicated slopes and y-intercepts are lines of best fit during the period of maximum rate of spindle elongation. Each data point represents a single cell. n=25-26; p values were determined using a two-tailed unpaired t test (*** = p<0.0001). Middle: Spindle length at anaphase onset. Each data point represents an individual cell. Median and the 95% confidence interval are shown. n=25-26. Right: Calculated maximum rates of spindle elongation over a 2-minute period for each individual cell. Each data point represents a single cell. Median and the 95% confidence interval are shown. n=25-26; p values were determined using a two-tailed unpaired t test (*** = p<0.0001).

Figure 1 supplement. Conservation of the entire basic linker region of Stu2 across 9 fungal species as well as viability assays of various mutants within Stu2$^{592-606}$.

(A) Top: Schematic of Stu2's domains as in Figure 1A. Bottom: Multiple sequence alignment across 9 different fungal species of Stu2's entire basic linker region. Note: numbers listed correspond to *S. cerevisiae* amino acid positions.

(B) Cell viability was analyzed in a wild-type strain (M3) as well as *stu2-AID* strains without a covering allele (M619) or ectopically expressing Stu2 (*STU2*^{WT}, M622; *stu2*$^{\Delta BL}$, M973; *stu2*$^{\Delta 592-606}$, M852; or *stu2*$^{\Delta 633-648}$, M851) by plating five-fold serial dilutions in the presence of DMSO (left) or auxin (right) to degrade the endogenous Stu2-AID protein. Note: we observed two patches of conservation within the basic linker domain, 592-606 (containing 3 Lys and Arg residues) and 633-648 (containing 4 Lys and Arg residues). Deletion of 592-606 displayed severe growth defects, whereas deletion of 633-648 showed no growth defect.

(C) Cell viability was analyzed in *stu2-AID* strains without a covering allele (M619) or ectopically expressing Stu2 (*STU2*^{WT}, M622; *stu2*^{K598A}, M954; *stu2*^{R599A}, M956; or *stu2*$^{KR/AA}$, M888) by plating five-fold serial dilutions in the presence of DMSO (left) or auxin (right) to degrade the endogenous Stu2-AID protein. Here we observe that the *stu2*$^{KR/AA}$ mutant displays similar viability defects as the two single mutants.

(D) Cell viability was analyzed in *stu2-AID* strains without a covering allele (M619) or ectopically expressing Stu2 (*STU2*^{WT}, M622; *stu2*^{P596A}, M1290; *stu2*^{S597A}, M1299; *stu2*^{K598A}, M954; *stu2*^{R599A}, M956; *stu2*$^{V600A\ S602A}$, M1383; or *stu2*^{S603A}, M802) by plating five-fold serial dilutions in the presence of 6.5 µg/mL benomyl with DMSO (left) or auxin (right) to degrade the endogenous Stu2-AID protein. On plates containing benomyl and auxin, cells expressing *stu2*^{P596A} display viability defects.

(E) Cell viability was analyzed in a wild-type strain (M3) as well as *stu2-AID* strains without a covering allele (M619) or ectopically expressing Stu2 variants (*stu2*$^{\Delta BL::592-606}$*, i.e. STU2*^{WT},

M991; *stu2*$^{\Delta BL::592\text{-}606(S592A\ S593A\ V594A\ L595A)}$, M1519; or *stu2*$^{\Delta BL::592\text{-}606(P604A\ L605A\ R606A)}$, M1518) by plating five-fold serial dilutions in the presence of DMSO (left) or auxin and DMSO (right) to degrade the endogenous Stu2-AID protein.

(F) Spore viability was analyzed from a sporulated diploid strain (M1265) with a heterozygous deletion of *stu2* at the endogenous *STU2* locus (*STU2*/*stu2Δ*) and homozygous *stu2*$^{KR/AA}$/*stu2*$^{KR/AA}$ expressed from the *LEU2* locus. Individual haploid spores were isolated by tetrad dissection and grown on YPD. Each column of four spores are from a single dissected tetrad. Red boxes indicate the location of a spore that contains *stu2Δ* at the endogenous *STU2* locus and *stu2*$^{KR/AA}$ at the *LEU2* locus. Lack of colony formation indicates viability defects, consistent with Stu2$^{K598\ R599}$ being critical residues for *S. cerevisiae* viability.

Figure 2 supplement. Characterization of basic linker mutants' ability to form a mitotic spindle and regulate microtubule dynamics.

(A) Exponentially growing *SPC110-mCherry stu2-AID cdc20-AID* cells ectopically expressing *STU2* (*STU2*^{WT}, M1914; *stu2*$^{\Delta BL}$, M1918; *stu2*$^{\Delta 592\text{-}606}$, M1921; or *stu2*$^{KR/AA}$, M1922) were treated with auxin for 2 hours to degrade Stu2-AID and arrest cells in metaphase. Cells were fixed and the Spc110-mCherry signal was imaged. Left: proportion of cells with non-separated spindle pole bodies vs a short spindle (less than the 1st quartile spindle length for cells expressing *STU2*^{WT}) vs a normal length spindle (greater than the 1st quartile spindle length for cells expressing *STU2*^{WT}) were determined. n = 102-118 cells. Right: representative cell with varying spindle lengths.

(B) Representative kymograph images for individual microtubule extensions grown from cell lysates harvested from each of the strains in the experiment from Fig. 2C (no covering allele, M2166; *STU2*^{WT}, M2231; *stu2*$^{\Delta BL}$, M2360; *stu2*$^{\Delta 592\text{-}606}$, M2234; or *stu2*$^{KR/AA}$, M2232). These kymographs show microtubule extension (red) from the microtubule seed (teal) over time.

(C) Exponentially growing *GFP-TUB1 stu2-AID cdc23-1* cells with no covering allele (M2166) or ectopically expressing Stu2 (*STU2*^{WT}, M2231; *stu2*$^{\Delta BL}$, M2360; *stu2*$^{\Delta 592\text{-}606}$, M2234; or *stu2*$^{KR/AA}$, M2232) were shifted to a non-permissive temperature for 3 hours to arrest cells in metaphase and treated with auxin for 30 minutes to degrade Stu2-AID. Whole cell lysate was incubated with microtubule seeds, and growth and shrinkage rates of microtubule extensions were determined. Dynamics of microtubules were also determined, and the average percent time that a microtubule was in a state of growth versus shrinkage versus paused are indicated for each.

(D) Microtubule catastrophe frequencies were determined from Stu2 variant samples as described in Fig S2C, kymograph images as shown in S2B. Note: catastrophe frequency increases by approximately 3.2-fold from no covering allele to *STU2*^{WT}, while there is no significant difference between no covering allele and *stu2*$^{\Delta BL}$. This suggests the basic linker of Stu2 is important in promoting catastrophe of microtubules.

(E) Microtubule rescue frequency of cells shown above in S2C was determined from kymograph images as shown in S2B.

(F) Representative kymographs for αβ-tubulin alone, +Stu2^{WT} and +Stu2$^{KR/AA}$ respectively. +Stu2^{WT} as shown in Fig. 2D. Microtubule dynamics were measured by time-lapse DIC microscopy.

Figure 3 supplement. Ratio of nuclear to cytoplasmic GFP signal intensity in Stu2$^{592-607}$-GFP-GST with a copy of GFP that is unable to dimerize.

Exponentially growing *stu2-AID cdc20-AID* cells ectopically expressing GFP-GST fusion constructs (Stu2$^{592-607}$-GFP-GST, M2392; or Stu2$^{592-607}$-GFP(A206K)-GST, M2480) were treated with auxin for 2 hours to degrade Stu2-AID and arrest cells in metaphase. Cells were fixed and Nup2-mKATE and GFP signals were imaged and the ratio of nuclear to cytoplasmic GFP signal intensities was quantified. Each data point represents this ratio for a single cell. Median and the 95% confidence interval are shown. n=116-122 cells; p values were determined using a two-tailed unpaired t test (*** = p<0.0001). Here we find that using a copy of GFP that is unable to homodimerize, as shown in (Zacharias et al., 2002), does not alter the nuclear to cytoplasmic GFP ratio of Stu2$^{592-607}$-GFP-GST, suggesting that the conserved patch (Stu2$^{592-607}$) does not need to be a dimer for nuclear localization function.

Figure 4 supplement. Cell cycle dependent regulation of nuclear import of Stu2$^{592-607}$-GFP-GST and specifically the effects of phosphorylation deficient and phosphorylation mimicking mutations of Stu2^{S603}.

(A) Exponentially growing *stu2-AID* cells with or without *cdc20-AID* and ectopically expressing Stu2$^{592-607}$-GFP-GST were either treated with auxin for 2 hours to degrade Stu2-AID and Cdc20-AID to arrest cells in metaphase (M2392) or treated with α-factor for 2.5 hours to arrest cells in G1 and then auxin for 30 minutes to degrade Stu2-AID (M2443). Cells were fixed and Nup2-mKATE and Stu2$^{592-607}$-GFP-GST signals were imaged. The ratios of nuclear to cytoplasmic GFP intensities were quantified. Each data point represents this ratio for a single cell. Median and the 95% confidence interval are shown. n=111-143 cells; p values were determined using a two-tailed unpaired t test (*** = p<0.0001).

(B) Exponentially growing *stu2-AID cdc20-AID* cells ectopically expressing a GFP-GST fusion construct (Stu2$^{592-607}$, M2392; Stu2$^{592-607(S603A)}$, M2438; Stu2$^{592-607(S603E)}$, M2726; or Stu2$^{592-607(KR/AA)}$, M2437) were treated with auxin for 2 hours to degrade Stu2-AID and Cdc20-AID to arrest cells in metaphase. Cells were fixed and Nup2-mKATE and GFP signals were imaged. The ratios of nuclear to cytoplasmic GFP intensities were quantified. Each data point represents this ratio for a single cell. Median and the 95% confidence interval are shown. n=104-124 cells; p values were determined using a two-tailed unpaired t test (*** = p<0.0001).

Note: the S603A mutant shows a greater mitotic nuclear to cytoplasmic GFP intensity ratio compared to Stu2$^{592-607(KR/AA)}$-GFP-GST (0.81 +/- 0.03 versus 0.67 ± 0.02), suggesting S603A does not entirely disrupt the nuclear localization function of Stu2$^{592-607}$.

Figure 5 supplement. Modulating nuclear levels of Stu2$^{KR/AA}$ affects viability, and the basic linker domain is required for Stu2's ability to stimulate microtubule assembly and disassembly in vitro, but is dispensable for cell viability as long as Stu2 is localized to the nucleus.

(A) Schematic of Stu2 domains indicating mutated residues in the experimental strains used in B.

(B) Cell viability was analyzed in a wild-type strain (M3) as well as *stu2-AID* strains without a covering allele (M619) or ectopically expressing *STU2* (*STU2*^{WT}, M2103; *stu2*$^{S813A\ S815A}$, M2248; *stu2*$^{S813D\ S815D}$, M2249; *stu2*$^{KR/AA\ S813A\ S815A}$, M2250; *stu2*$^{KR/AA\ S813D\ S815D}$, M2251; or *stu2*$^{KR/AA}$, M2225) by plating five-fold serial dilutions in the presence of DMSO (left) or auxin (right) to degrade the endogenous Stu2-AID protein.

(C) Cell viability was analyzed in a wild-type strain (M3) as well as *stu2-AID* strains without a covering allele (M619) or ectopically expressing *STU2* (*STU2*^{WT}, M622; *stu2*$^{\Delta BL}$, M973; *stu2*$^{\Delta BL::592-606}$, M991; *stu2*$^{\Delta BL::596-604}$, M1710; *stu2*$^{\Delta BL::596-599}$, M1301) by plating five-fold serial dilutions in the presence of DMSO (left) or auxin (right) to degrade the endogenous Stu2-AID protein.

(D) Exponentially growing *GFP-TUB1 stu2-AID cdc23-1* cells with no covering allele (M2166) or ectopically expressing Stu2-Halo (*STU2*^{WT}, M2231; *stu2*$^{\Delta BL}$, M2360; or *stu2*$^{\Delta BL}$-*NLS*^{SV40}, M3516) were shifted to a non-permissive temperature for 3 hours to arrest cells in metaphase and treated with auxin for 30 minutes to degrade Stu2-AID. Whole cell lysate was incubated with microtubule seeds, and growth and shrinkage rates of microtubule extensions were determined. Left: Representative kymographs (red, microtubule extension; cyan, seed; no covering allele, *STU2*^{WT}, and *stu2*$^{\Delta BL}$ as shown in Fig. S2B). Rates of microtubule assembly or disassembly are determined by the slope of microtubule extension growth and shrinkage over time. Top right: Assembly rates of microtubules. Each data point represents an independent microtubule assembly event. Median and the 95% confidence interval are shown. n=182-398 growth events. Bottom right: Disassembly rates of microtubules. Each data point represents an independent microtubule disassembly event. Median and the 95% confidence interval are shown. n=21-181 shrinkage events; p values were determined using a two-tailed unpaired t test (**** = $p<0.0001$).

(E) Exponentially growing *stu2-AID* strains without a covering allele (M2166) or ectopically expressing *STU2-Halo-3V5* alleles (*STU2*^{WT}, M2231; *stu2*$^{\Delta BL}$, M2360; or *stu2*$^{\Delta BL}$-*NLS*^{SV40}, M3516) were harvested, and protein lysates were subsequently prepared and expression of Stu2-3V5 proteins were analyzed by immunoblotting. Pgk1 is shown as a loading control.

(F) Cell viability was analyzed in *stu2-AID* strains without a covering allele (M2166) or ectopically expressing *STU2-Halo-3V5* alleles (*STU2*^{WT}, M2231; *stu2*$^{\Delta BL}$, M2360; or *stu2*$^{\Delta BL}$-*NLS*^{SV40}, M3516) by plating five-fold serial dilutions in the presence of DMSO (left) or auxin (right) to degrade the endogenous Stu2-AID protein.

Figure 1

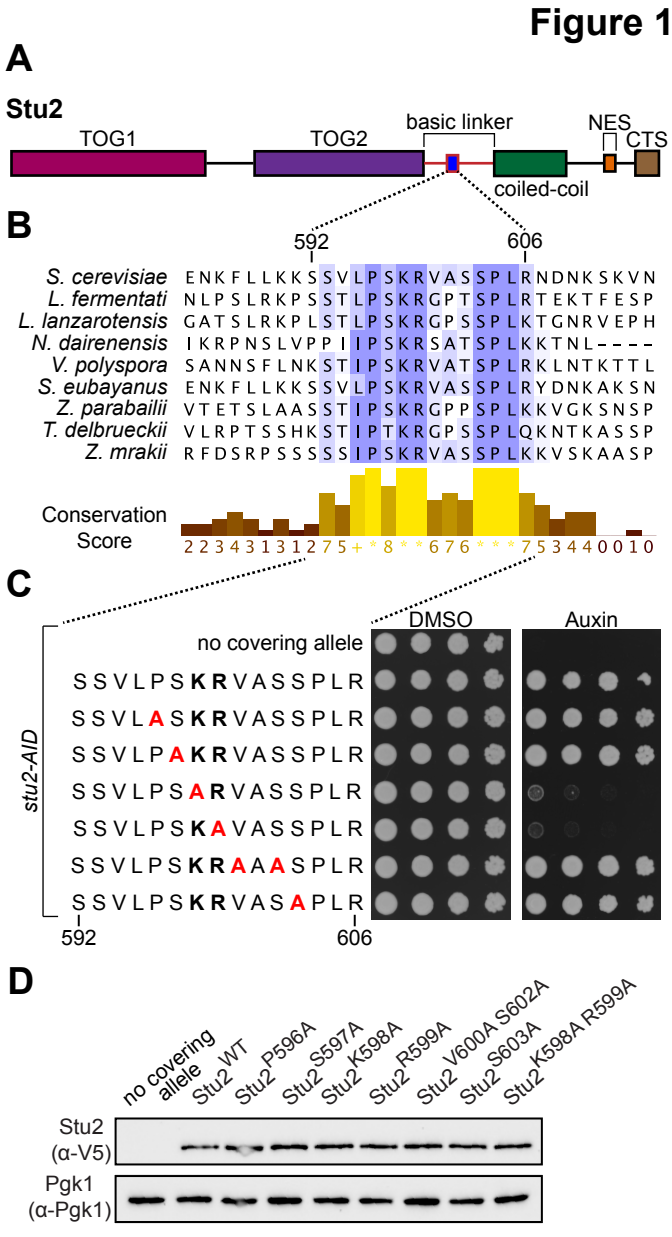
A
Stu2
TOG1
TOG2
basic linker
NES
CTS
coiled-coil
B
592
606
S. cerevisiae ENKFLLKKSSVLPSKRVASSPLRNDNKSKVN
L. fermentati NLPSLRKPSSTLPSKRGPTSPLRTEKTFESP
L. lanzarotensis GATSLRKPLSTLPSKRGPSSPLKTGNRVEPH
N. dairenensis IKRPNSLVPPIIPSKRSATSPLKKTNL----
V. polyspora SANNSFLNKSTIPSKRVATSPLRKLNTKTTL
S. eubayanus ENKFLLKKSSVLPSKRVASSPLRYDNKAKSN
Z. parabailii VTETSLAASSTIPSKRGPPSPLKKVGKSNSP
T. delbrueckii VLRPTSSHKSTIPTKRGPSSPLQKNTKASSP
Z. mrakii RFDSRPSSSSSIPSKRVASSPLKKVSKAASP
Conservation Score
2 2 3 4 3 1 3 1 2 7 5 + * 8 * * 6 7 6 * * * 7 5 3 4 4 0 0 1 0
C
DMSO
Auxin
no covering allele
stu2-AID
SSVLPSKRVASSPLR
SSVLASKRVASSPLR
SSVLPAKRVASSPLR
SSVLPSARVASSPLR
SSVLPSKAVASSPLR
SSVLPSKRAAASPLR
SSVLPSKRVASAPLR
592
606
D
no covering allele
Stu2 WT
Stu2 P596A
Stu2 S597A
Stu2 K598A
Stu2 R599A
Stu2 V600A S602A
Stu2 S603A
Stu2 K598A R599A
Stu2 (α-V5)
Pgk1 (α-Pgk1)

Figure 2

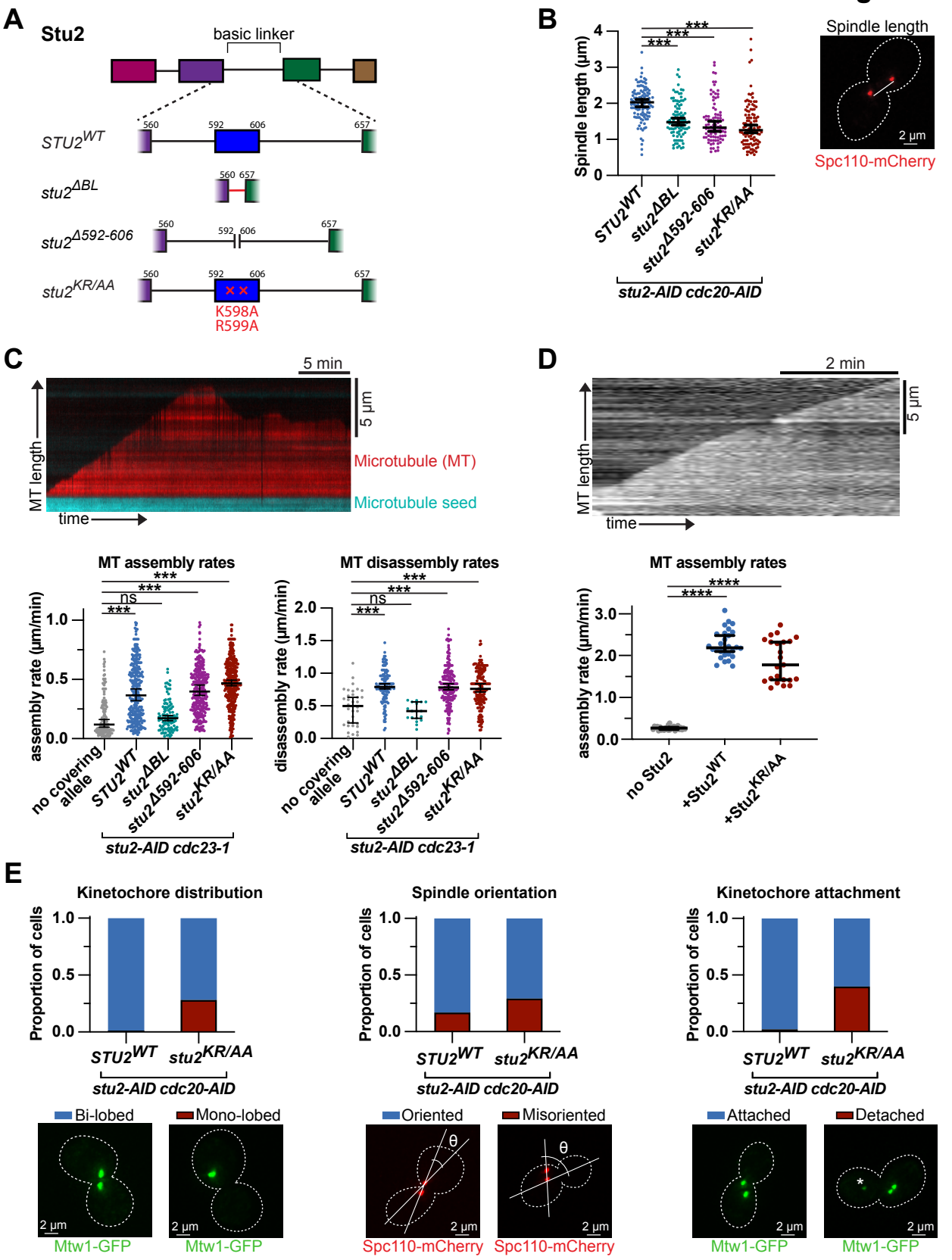
A
Stu2
basic linker
STU2WT
560
592
606
657
stu2ΔBL
stu2Δ592-606
stu2KR/AA
K598A
R599A
B
Spindle length (µm)
STU2WT
stu2ΔBL
stu2Δ592-606
stu2KR/AA
stu2-AID cdc20-AID
Spindle length
2 µm
Spc110-mCherry
C
5 min
5 µm
MT length
time
Microtubule (MT)
Microtubule seed
MT assembly rates
assembly rate (µm/min)
no covering allele
stu2-AID cdc23-1
MT disassembly rates
disassembly rate (µm/min)
D
2 min
MT assembly rates
assembly rate (µm/min)
no Stu2
+Stu2WT
+Stu2KR/AA
E
Kinetochore distribution
Spindle orientation
Kinetochore attachment
Proportion of cells
stu2-AID cdc20-AID
Bi-lobed
Mono-lobed
Oriented
Misoriented
Attached
Detached
Mtw1-GFP
Spc110-mCherry

Figure 3

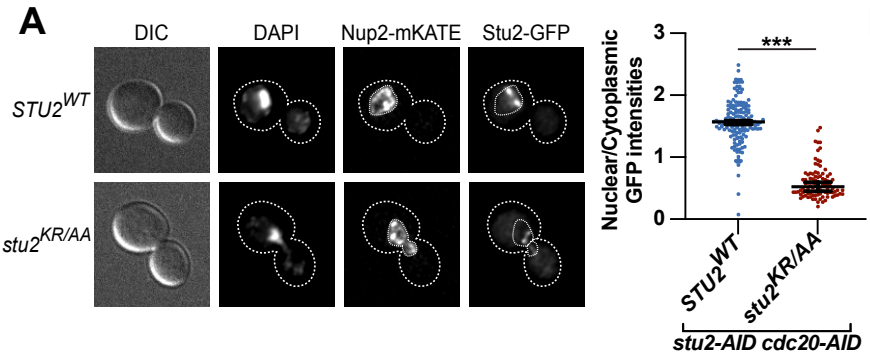
A
DIC
DAPI
Nup2-mKATE
Stu2-GFP
STU2WT
stu2KR/AA
Nuclear/Cytoplasmic GFP intensities
3
2
1
0
***
STU2WT
stu2KR/AA
stu2-AID cdc20-AID

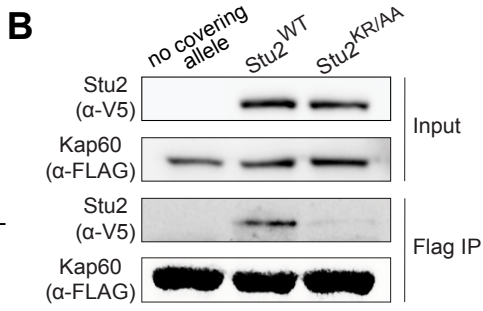
B
no covering allele
Stu2WT
Stu2KR/AA
Stu2 (α-V5)
Kap60 (α-FLAG)
Input
Stu2 (α-V5)
Kap60 (α-FLAG)
Flag IP

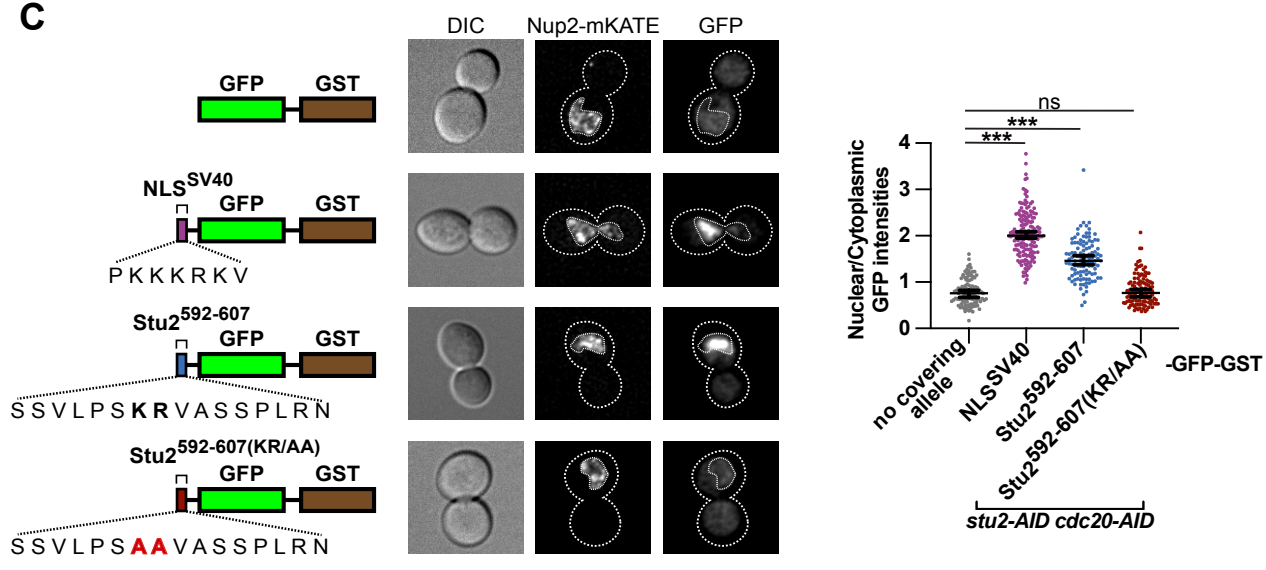
C
DIC
Nup2-mKATE
GFP
GFP
GST
NLSSV40
GFP
GST
P K K K R K V
Stu2592-607
GFP
GST
S S V L P S K R V A S S P L R N
Stu2592-607(KR/AA)
GFP
GST
S S V L P S A A V A S S P L R N
Nuclear/Cytoplasmic GFP intensities
4
3
2
1
0
ns
***
***
no covering allele
NLSSV40
Stu2592-607
Stu2592-607(KR/AA)
-GFP-GST
stu2-AID cdc20-AID

Figure 4

A

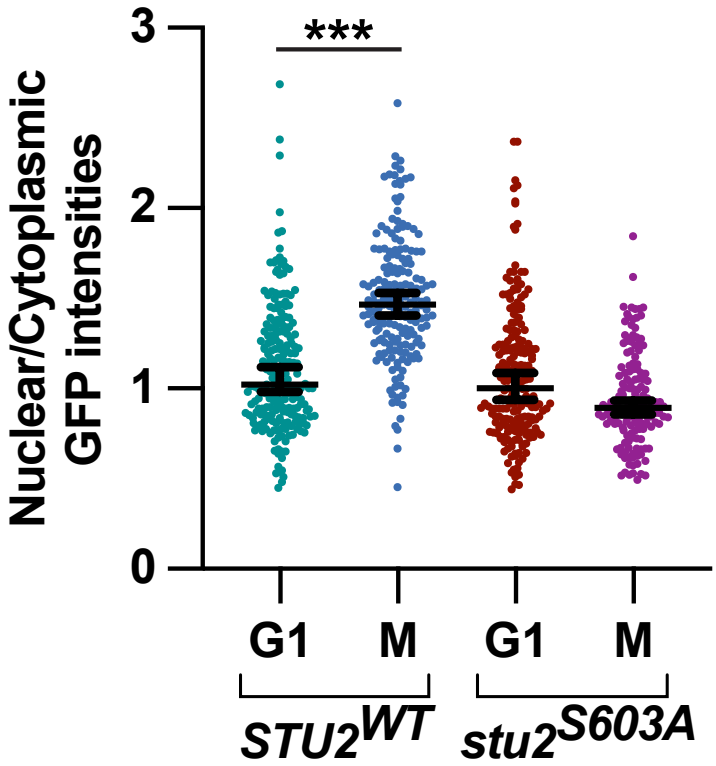
Nuclear/Cytoplasmic GFP intensities
3
2
1
0
***
G1
M
G1
M
STU2WT
stu2S603A

B

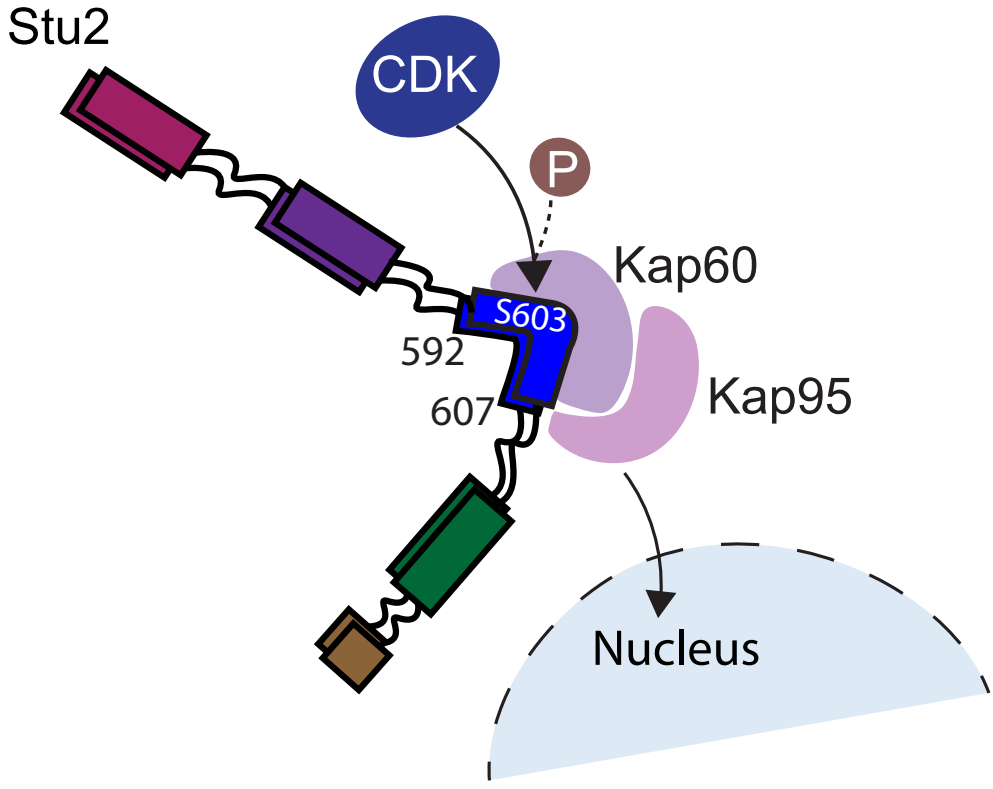
Stu2
CDK
P
Kap60
S603
592
607
Kap95
Nucleus

Figure 5

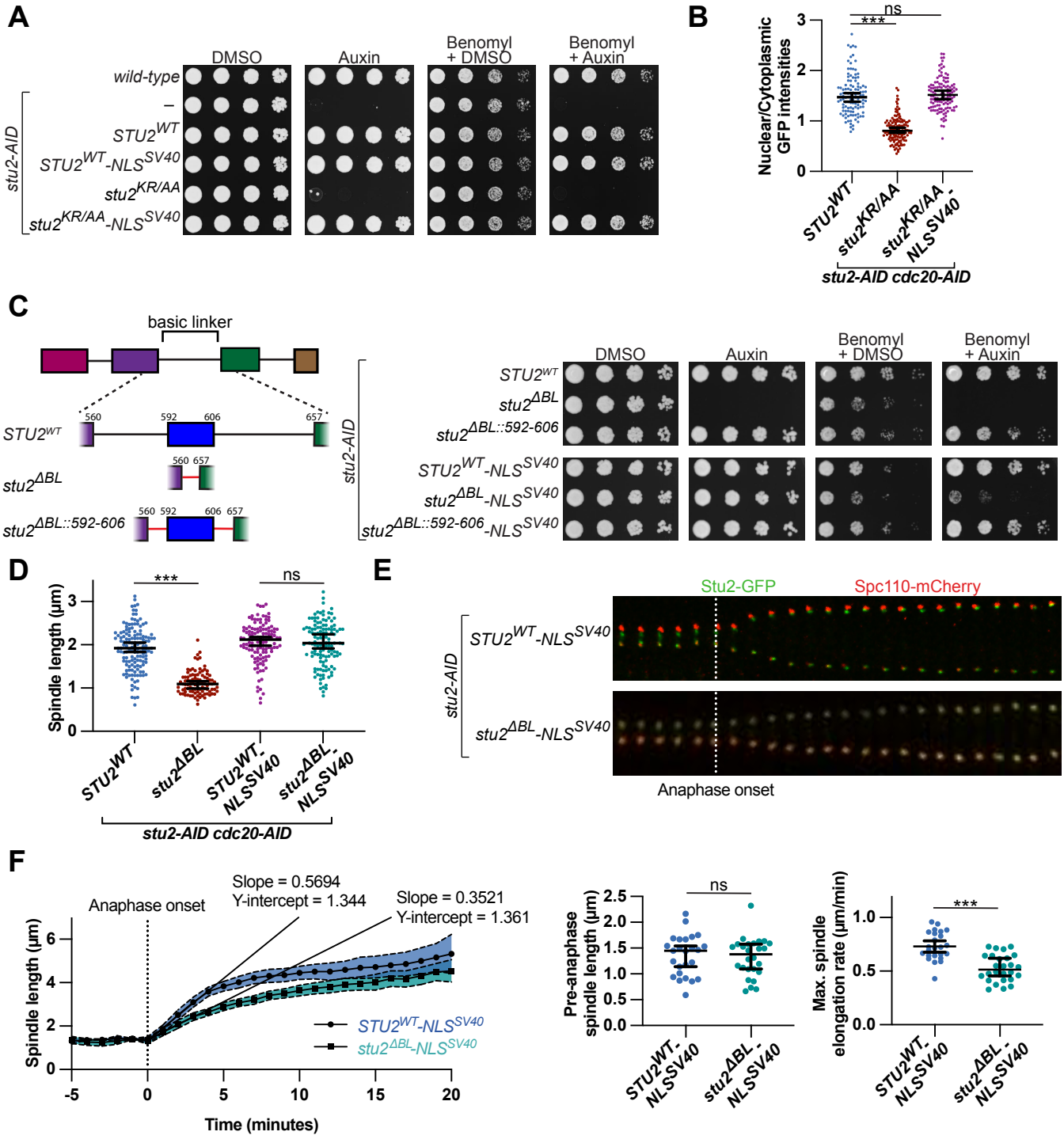
A
DMSO
Auxin
Benomyl + DMSO
Benomyl + Auxin
wild-type
–
STU2WT
STU2WT-NLSSV40
stu2KR/AA
stu2KR/AA-NLSSV40
stu2-AID
B
Nuclear/Cytoplasmic GFP intensities
ns
***
STU2WT
stu2KR/AA
stu2KR/AA-NLSSV40
stu2-AID cdc20-AID
C
basic linker
STU2WT
560
592
606
657
stu2ΔBL
stu2ΔBL::592-606
stu2-AID
STU2WT-NLSSV40
stu2ΔBL-NLSSV40
stu2ΔBL::592-606-NLSSV40
D
Spindle length (µm)
STU2WT
stu2ΔBL
STU2WT-NLSSV40
stu2ΔBL-NLSSV40
stu2-AID cdc20-AID
E
Stu2-GFP
Spc110-mCherry
Anaphase onset
F
Anaphase onset
Slope = 0.5694
Y-intercept = 1.344
Slope = 0.3521
Y-intercept = 1.361
Spindle length (µm)
Time (minutes)
Pre-anaphase spindle length (µm)
Max. spindle elongation rate (µm/min)

Figure S1

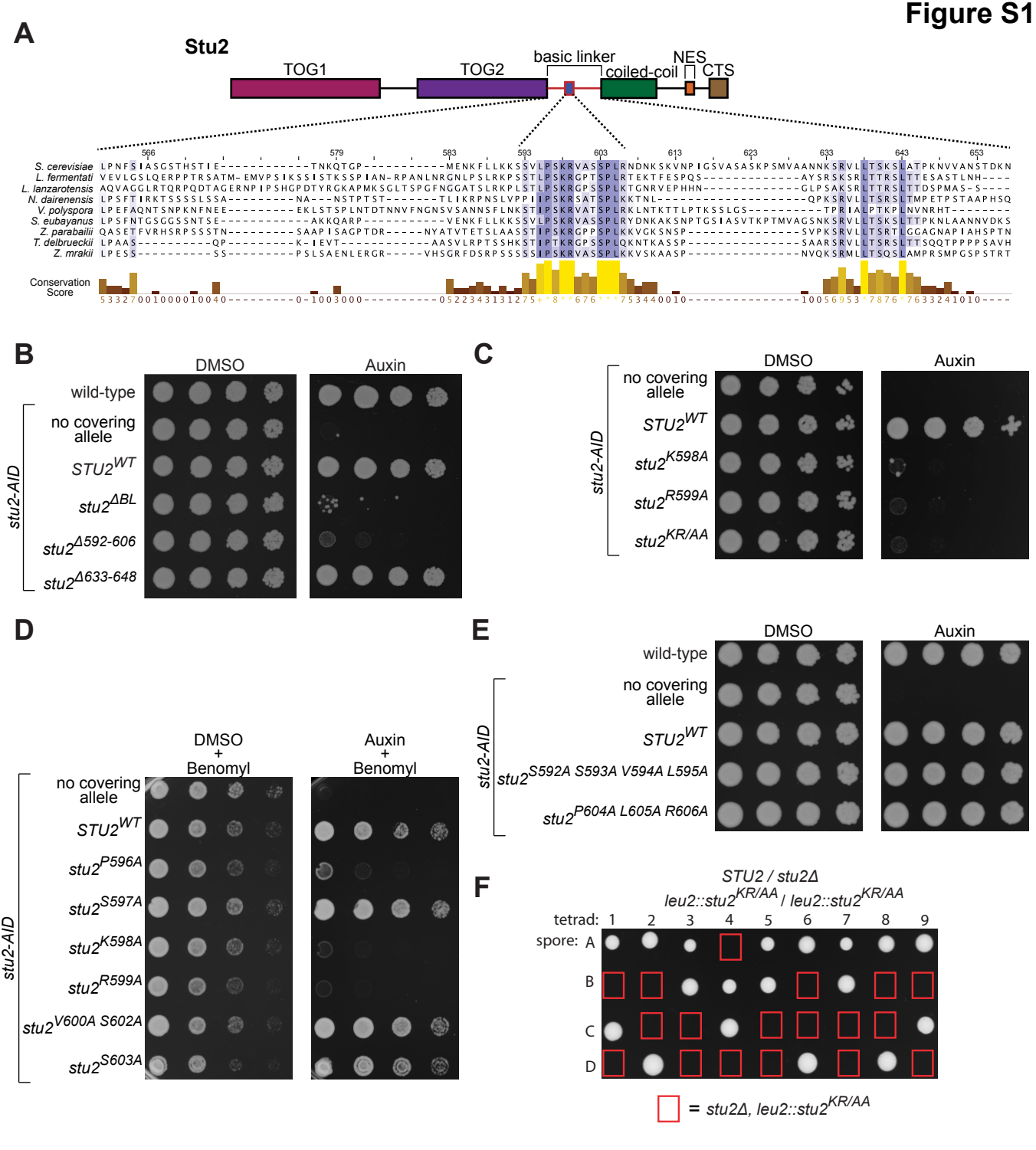
A
Stu2
TOG1
TOG2
basic linker
coiled-coil
NES
CTS
S. cerevisiae
L. fermentati
L. lanzarotensis
N. dairenensis
V. polyspora
S. eubayanus
Z. parabailii
T. delbrueckii
Z. mrakii
Conservation Score
B
DMSO
Auxin
wild-type
no covering allele
STU2WT
stu2ΔBL
stu2Δ592-606
stu2Δ633-648
stu2-AID
C
DMSO
Auxin
no covering allele
STU2WT
stu2K598A
stu2R599A
stu2KR/AA
stu2-AID
D
DMSO + Benomyl
Auxin + Benomyl
no covering allele
STU2WT
stu2P596A
stu2S597A
stu2K598A
stu2R599A
stu2V600A S602A
stu2S603A
stu2-AID
E
DMSO
Auxin
wild-type
no covering allele
STU2WT
stu2S592A S593A V594A L595A
stu2P604A L605A R606A
stu2-AID
F
STU2 / stu2Δ
leu2::stu2KR/AA / leu2::stu2KR/AA
tetrad: 1 2 3 4 5 6 7 8 9
spore: A
B
C
D
= stu2Δ, leu2::stu2KR/AA

Figure S2

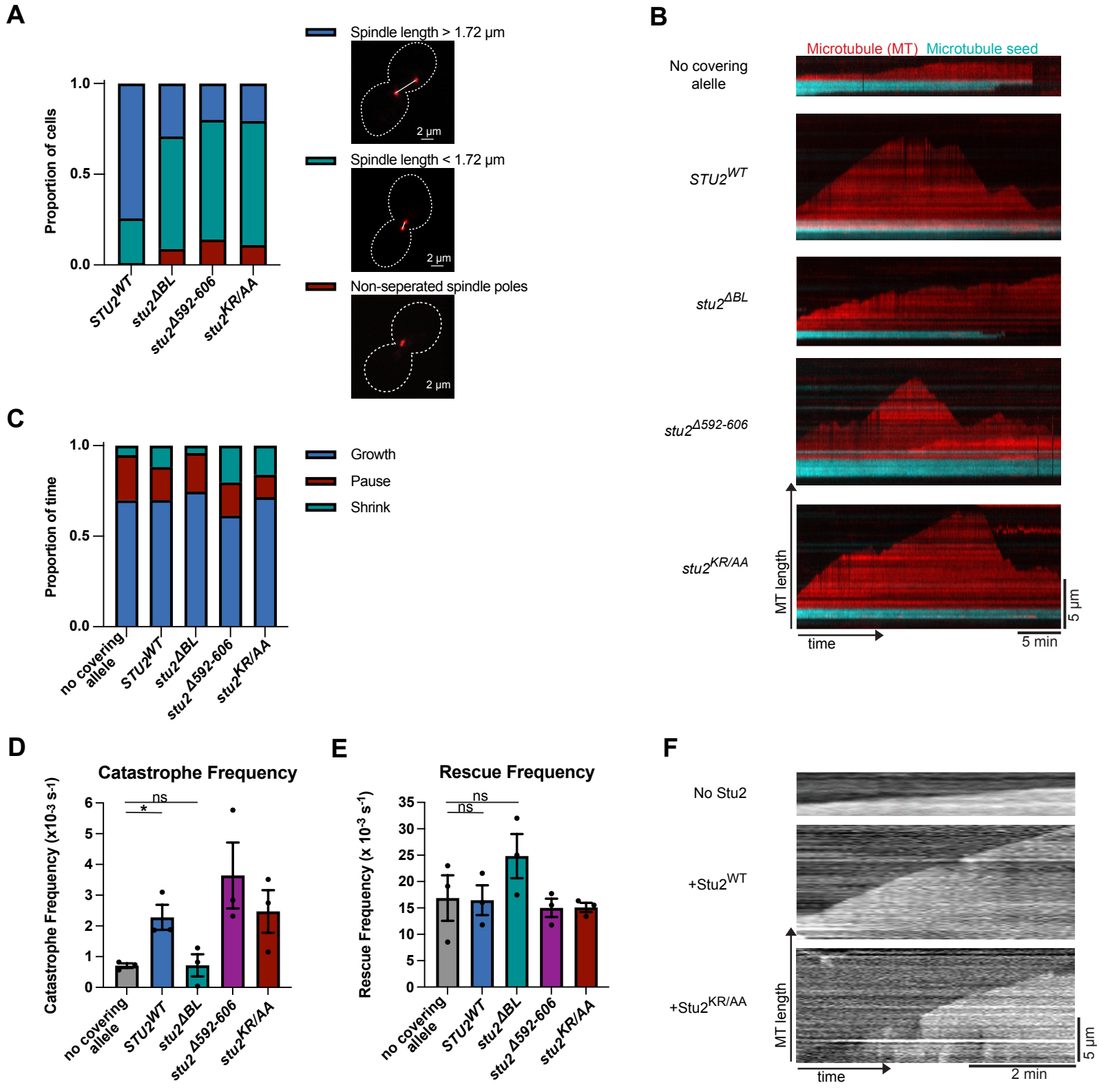
A
Spindle length > 1.72 µm
Spindle length < 1.72 µm
Non-seperated spindle poles
2 µm
Proportion of cells
1.0
0.5
0.0
STU2WT
stu2ΔBL
stu2Δ592-606
stu2KR/AA
B
Microtubule (MT)
Microtubule seed
No covering alelle
STU2WT
stu2ΔBL
stu2Δ592-606
stu2KR/AA
MT length
5 µm
time
5 min
C
Proportion of time
Growth
Pause
Shrink
no covering allele
D
Catastrophe Frequency
Catastrophe Frequency (x10-3 s-1)
ns
*
E
Rescue Frequency
Rescue Frequency (x 10-3 s-1)
F
No Stu2
+Stu2WT
+Stu2KR/AA
2 min

Figure S3

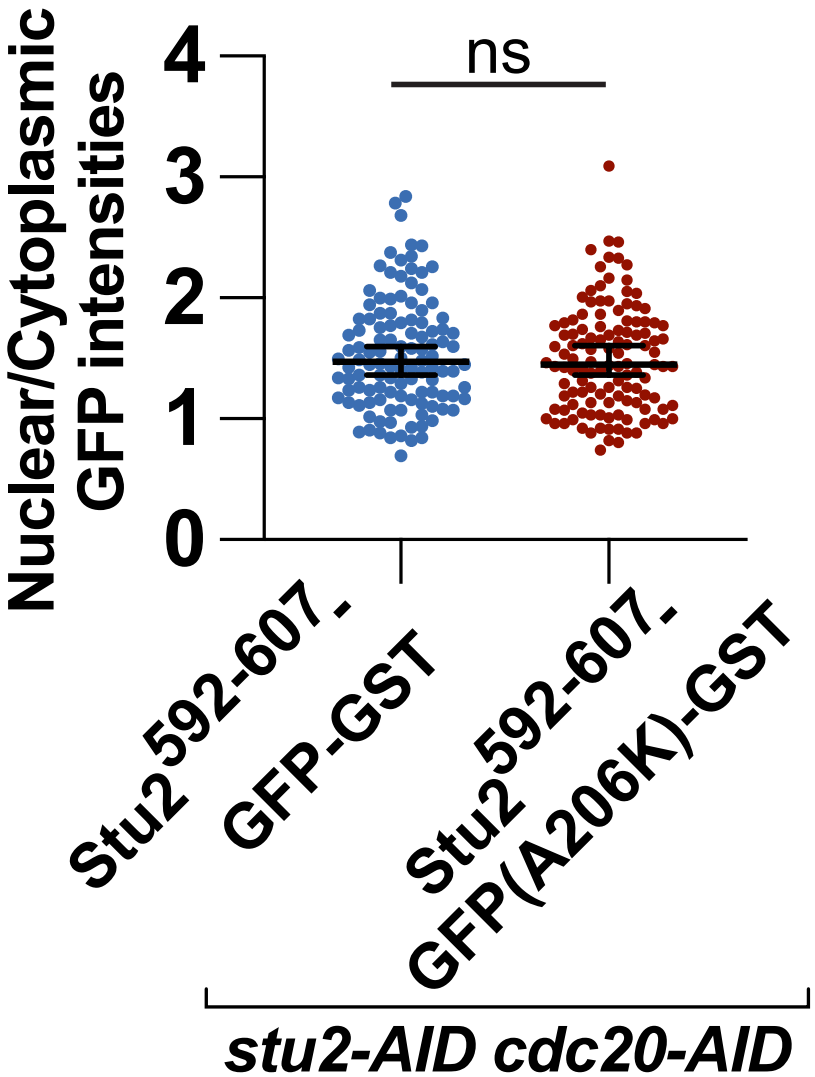
Nuclear/Cytoplasmic GFP intensities
4
3
2
1
0
ns
Stu2 592-607 - GFP-GST
Stu2 592-607 - GFP(A206K)-GST
stu2-AID cdc20-AID

Figure S4

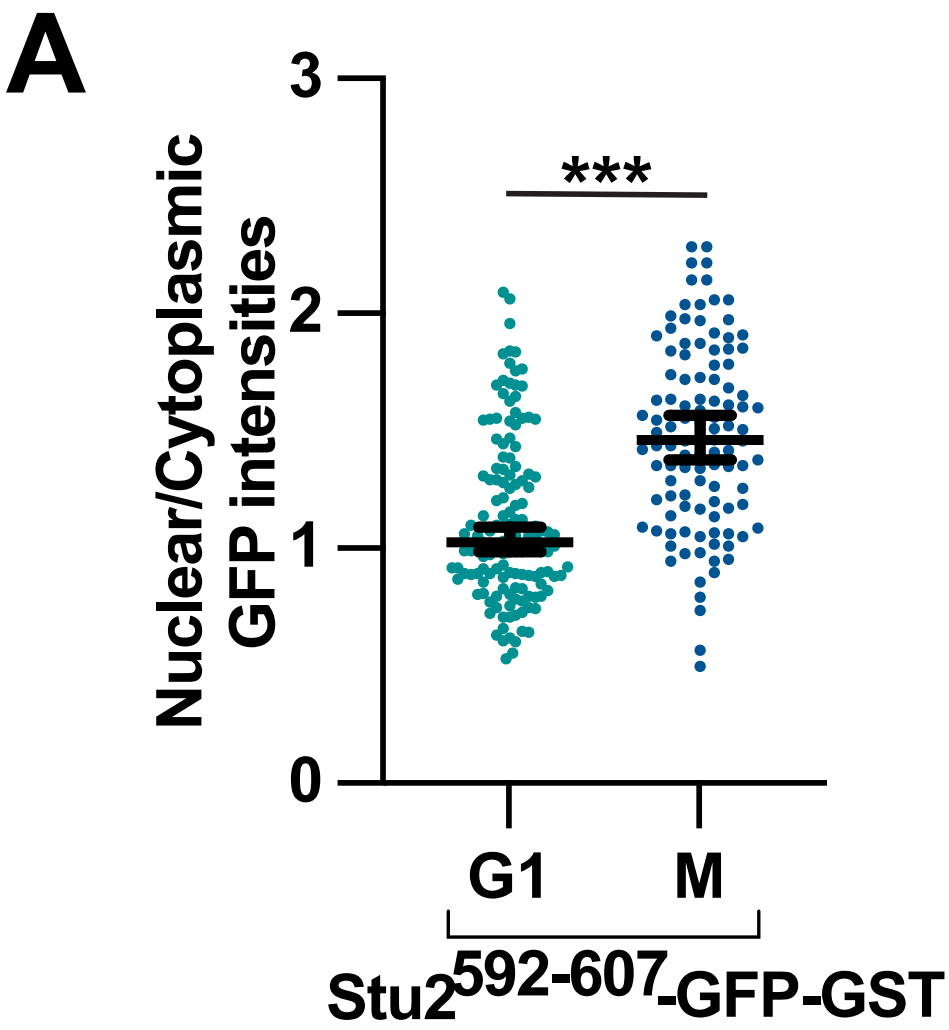
A
Nuclear/Cytoplasmic GFP intensities
3
2
1
0
***
G1
M
Stu2592-607-GFP-GST

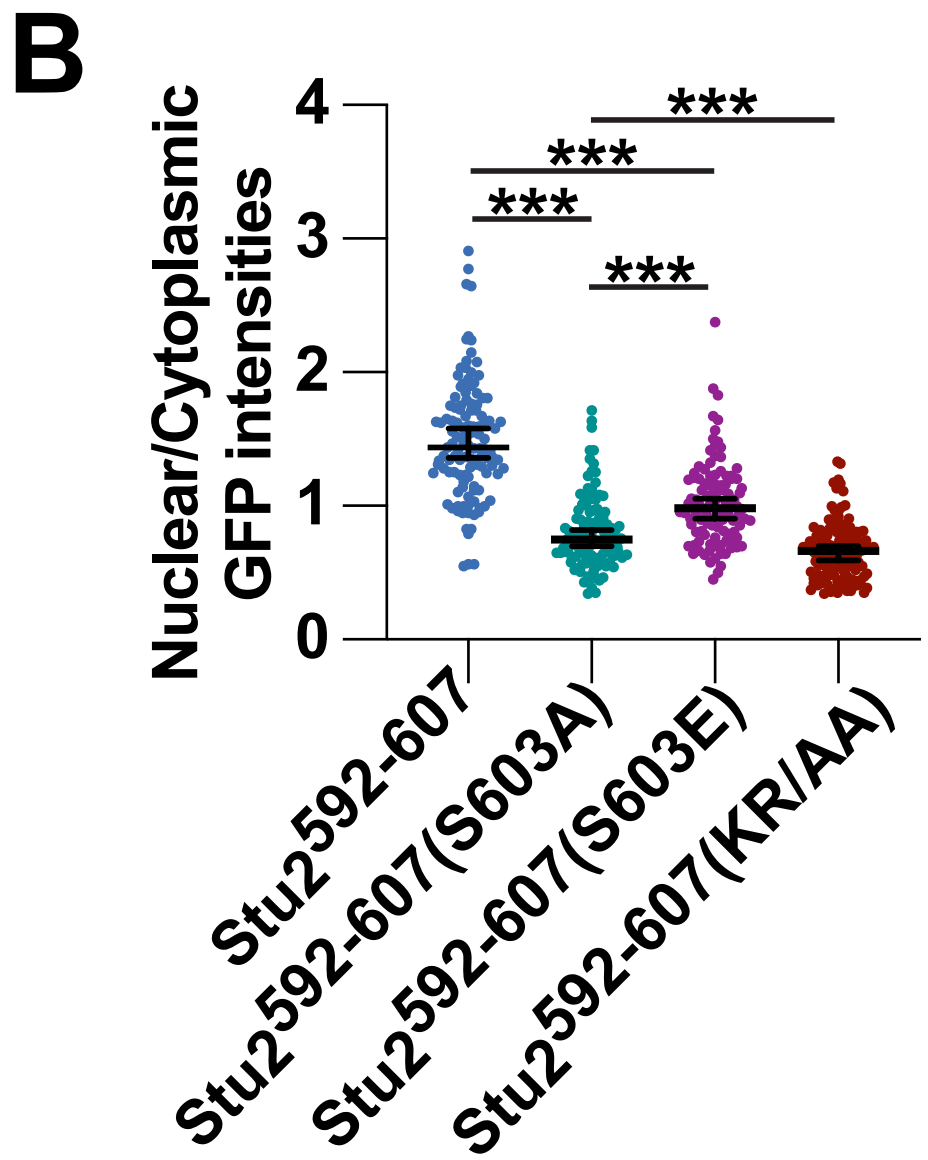
B
Nuclear/Cytoplasmic GFP intensities
4
3
2
1
0
***
***
***
***
Stu2592-607
Stu2592-607(S603A)
Stu2592-607(S603E)
Stu2592-607(KR/AA)

Figure S5

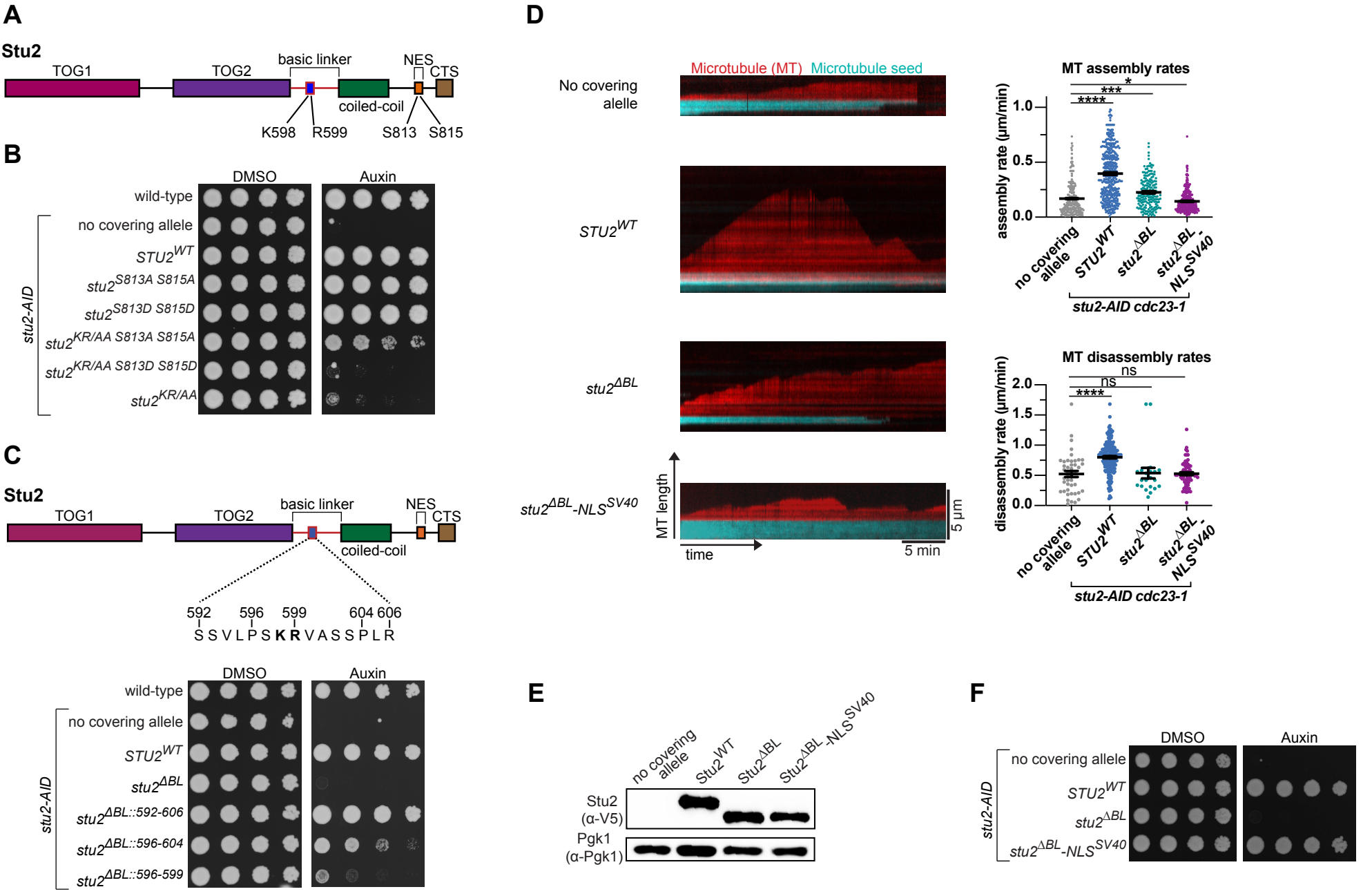
A
Stu2
TOG1
TOG2
basic linker
NES
CTS
coiled-coil
K598
R599
S813
S815
B
DMSO
Auxin
wild-type
no covering allele
STU2WT
stu2S813A S815A
stu2S813D S815D
stu2KR/AA S813A S815A
stu2KR/AA S813D S815D
stu2KR/AA
stu2-AID
C
Stu2
TOG1
TOG2
basic linker
NES
CTS
coiled-coil
592 596 599 604 606
S S V L P S K R V A S S P L R
DMSO
Auxin
wild-type
no covering allele
STU2WT
stu2ΔBL
stu2ΔBL::592-606
stu2ΔBL::596-604
stu2ΔBL::596-599
stu2-AID
D
Microtubule (MT)
Microtubule seed
No covering alelle
STU2WT
stu2ΔBL
stu2ΔBL-NLSSV40
MT length
time
5 µm
5 min
MT assembly rates
assembly rate (µm/min)
1.0
0.5
0.0
****
***
*
no covering allele
STU2WT
stu2ΔBL
stu2ΔBL-NLSSV40
stu2-AID cdc23-1
MT disassembly rates
disassembly rate (µm/min)
2.0
1.5
1.0
0.5
0.0
ns
****
no covering allele
STU2WT
stu2ΔBL
stu2ΔBL-NLSSV40
stu2-AID cdc23-1
E
no covering allele
Stu2WT
Stu2ΔBL
Stu2ΔBL-NLSSV40
Stu2 (α-V5)
Pgk1 (α-Pgk1)
F
DMSO
Auxin
no covering allele
STU2WT
stu2ΔBL
stu2ΔBL-NLSSV40
stu2-AID

Supplementary Table 1A. Strains used in this study that are derivatives of M3 (W303).

Strain	Relevant Genotype
M3 (W303)	*MAT**a** ura3-1 leu2-3,112 his3-11 trp1-1 can1-100 ade2-1 bar1-1*
M619	*MAT**a** his3::pGPD1-OsTIR1:HIS3 stu2-3HA-IAA7:KanMX DSN1-HIS-FLAG:URA3*
M622	*MAT**a** leu2::pSTU2-STU2-3V5:LEU2 his3::pGPD1-OsTIR1:HIS3 stu2-3HA-IAA7:KanMX DSN1-HIS-FLAG:URA3*
M802	*MAT**a** leu2::pSTU2-stu2(S603A)-3V5:LEU2 his3::pGPD1-OsTIR1:HIS3 stu2-3HA-IAA7:KanMX DSN1-HIS-FLAG:URA3*
M851	*MAT**a** leu2::pSTU2-stu2(Δ633-648)-3V5:LEU2 his3::pGPD1-OsTIR1:HIS3 stu2-3HA-IAA7:KanMX DSN1-HIS-FLAG:URA3*
M852	*MAT**a** leu2::pSTU2-stu2(Δ592-606)-3V5:LEU2 his3::pGPD1-OsTIR1:HIS3 stu2-3HA-IAA7:KanMX DSN1-HIS-FLAG:URA3*
M888	*MAT**a** leu2::pSTU2-stu2(K598A R599A)-3V5:LEU2 his3::pGPD1-OsTIR1:HIS3 stu2-3HA-IAA7:KanMX DSN1-HIS-FLAG:URA3*
M954	*MAT**a** leu2::pSTU2-stu2(K598A)-3V5:LEU2 his3::pGPD1-OsTIR1:HIS3 stu2-3HA-IAA7:KanMX DSN1-HIS-FLAG:URA3*
M956	*MAT**a** leu2::pSTU2-stu2(R599A)-3V5:LEU2 his3::pGPD1-OsTIR1:HIS3 stu2-3HA-IAA7:KanMX DSN1-HIS-FLAG:URA3*
M973	*MAT**a** leu2::pSTU2-stu2(Δ560-657::GDGAGL^{linker})-3V5:LEU2 his3::pGPD1-OsTIR1:HIS3 stu2-3HA-IAA7:KanMX DSN1-HIS-FLAG:URA3*
M991	*MAT**a** leu2::pSTU2-stu2(Δ560-657::GDGAGL^{linker}-(592-606)-GDGAGL^{linker})-3V5:LEU2 his3::pGPD1-OsTIR1:HIS3 stu2-3HA-IAA7:KanMX DSN1-HIS-FLAG:URA3*
M1265	*MAT**a**/MATα leu2::pSTU2-stu2(K598A R599A)-3V5:LEU2/leu2::pSTU2-stu2(K598A R599A)-3V5:LEU2, STU2/stu2Δ::TRP1*
M1290	*MAT**a** leu2::pSTU2-stu2(P596A)-3V5:LEU2 his3::pGPD1-OsTIR1:HIS3 stu2-3HA-IAA7:KanMX DSN1-HIS-FLAG:URA3*
M1299	*MAT**a** leu2::pSTU2-stu2(S597A)-3V5:LEU2 his3::pGPD1-OsTIR1:HIS3 stu2-3HA-IAA7:KanMX DSN1-HIS-FLAG:URA3*
M1301	*MAT**a** leu2::pSTU2-stu2(Δ560-657::GDGAGL^{linker}-(596-599)-GDGAGL^{linker})-3V5:LEU2 his3::pGPD1-OsTIR1:HIS3 stu2-3HA-IAA7:KanMX DSN1-HIS-FLAG:URA3*
M1383	*MAT**a** leu2::pSTU2-stu2(V600A S602A)-3V5:LEU2 his3::pGPD1-OsTIR1:HIS3 stu2-3HA-IAA7:KanMX DSN1-HIS-FLAG:URA3*
M1518	*MAT**a** leu2::pSTU2-stu2(Δ560-657::GDGAGL^{linker}-(592-606(P604A L605A R606A)-GDGAGL^{linker}))-3V5:LEU2 his3::pGPD1-OsTIR1:HIS3 stu2-3HA-IAA7:KanMX DSN1-HIS-FLAG:URA3*

M1519	*MAT**a** leu2::pSTU2-stu2(Δ560-657::GDGAGL^{linker}-(592-606(S592A S593A V594A L595A)-GDGAGL^{linker}))-3V5:LEU2 his3::pGPD1-OsTIR1:HIS3 stu2-3HA-IAA7:KanMX DSN1-HIS-FLAG:URA3*
M1710	*MAT**a** leu2::pSTU2-stu2(Δ560-657::GDGAGL^{linker}-(596-604)-GDGAGL^{linker})-3V5:LEU2 his3::pGPD1-OsTIR1:HIS3 stu2-3HA-IAA7:KanMX DSN1-HIS-FLAG:URA3*
M1757	*MAT**a** leu2::pSTU2-STU2-GFP:LEU2 trp1::pGPD1-OsTIR1:TRP1 cdc20-AID:KanMX SPC110-mCherry:HygMX stu2-3V5-IAA7:KanMX ura3-1::TUB1-CFP:URA3*
M1759	*MAT**a** leu2::pSTU2-stu2(Δ560-657)-GFP:LEU2 trp1::pGPD1-OsTIR1:TRP1 cdc20-AID:KanMX SPC110-mCherry:HygMX stu2-3V5-IAA7:KanMX ura3-1::TUB1-CFP:URA3*
M1914	*MAT**a** leu2::pSTU2-STU2-3V5:LEU2 trp1::pGPD1-OsTIR1:TRP1 cdc20-AID:KanMX SPC110-mCherry:HygMX stu2-3V5-IAA7:KanMX MTW1-3GFP:HIS3*
M1918	*MAT**a** leu2::pSTU2-stu2(Δ560-657:GDGAGL^{linker})-3V5:LEU2 trp1::pGPD1-OsTIR1:TRP1 cdc20-AID:KanMX SPC110-mCherry:HygMX stu2-3V5-IAA7:KanMX MTW1-3GFP:HIS3*
M1921	*MAT**a** leu2::pSTU2-stu2(Δ592-606)-3V5:LEU2 trp1::pGPD1-OsTIR1:TRP1 cdc20-AID:KanMX SPC110-mCherry:HygMX stu2-3V5-IAA7:KanMX MTW1-3GFP:HIS3*
M1922	*MAT**a** leu2::pSTU2-stu2(K598A R599A)-3V5:LEU2 trp1::pGPD1-OsTIR1:TRP1 cdc20-AID:KanMX SPC110-mCherry:HygMX stu2-3V5-IAA7:KanMX MTW1-3GFP:HIS3*
M2103	*MAT**a** leu2::pSTU2-STU2-GFP:LEU2 his3::pGPD1-OsTIR1:HIS3 stu2-3HA-IAA7:KanMX DSN1-HIS-FLAG:URA3*
M2105	*MAT**a** leu2::pSTU2-STU2-PKKKRKV$^{SV40\ NLS}$-GFP:LEU2 his3::pGPD1-OsTIR1:HIS3 stu2-3HA-IAA7:KanMX DSN1-HIS-FLAG:URA3*
M2107	*MAT**a** leu2::pSTU2-stu2(Δ560-657)-PKKKRKV$^{SV40\ NLS}$-GFP:LEU2 his3::pGPD1-OsTIR1:HIS3 stu2-3HA-IAA7:KanMX DSN1-HIS-FLAG:URA3*
M2125	*MAT**a** leu2::pSTU2-STU2-PKKKRKV$^{SV40\ NLS}$-GFP:LEU2 trp1::pGPD1-OsTIR1:TRP1 cdc20-AID:KanMX SPC110-mCherry:HygMX stu2-3V5-IAA7:KanMX ura3-1::TUB1-CFP:URA3*
M2126	*MAT**a** leu2::pSTU2-stu2(Δ560-657)-PKKKRKV$^{SV40\ NLS}$-GFP:LEU2 trp1::pGPD1-OsTIR1:TRP1 cdc20-AID:KanMX SPC110-mCherry:HygMX stu2-3V5-IAA7:KanMX ura3-1::TUB1-CFP:URA3*
M2199	*MAT**a** leu2::pSTU2-stu2(K598A R599A)-PKKKRKV$^{SV40\ NLS}$-GFP:LEU2 his3::pGPD1-OsTIR1:HIS3 stu2-3HA-IAA7:KanMX DSN1-HIS-FLAG:URA3*
M2208	*MAT**a** leu2::pSTU2-STU2-GFP:LEU2 stu2-3V5-IAA7:KanMX cdc20-AID:KanMX trp1::pGPD1-OsTIR1:TRP1 NUP2-mKATE2:HisMX6*
M2210	*MAT**a** leu2::pSTU2-stu2(K598A R599A)-GFP:LEU2 stu2-3V5-IAA7:KanMX cdc20-AID:KanMX trp1::pGPD1-OsTIR1:TRP1 NUP2-mKATE2:HisMX6*
M2217	*MAT**a** leu2::pSTU2-stu2(S603A)-GFP:LEU2 stu2-3V5-IAA7:KanMX cdc20-AID:KanMX trp1::pGPD1-OsTIR1:TRP1 NUP2-mKATE2:HisMX6*

M2225	*MAT**a** leu2::pSTU2-stu2(K598A R599A)-GFP:LEU2 his3::pGPD1-OsTIR1:HIS3 stu2-3HA-IAA7:KanMX DSN1-HIS-FLAG:URA3*
M2226	*MAT**a** leu2::pSTU2-stu2(Δ560-657:GDGAGL^{linker})-GFP:LEU2 his3::pGPD1-OsTIR1:HIS3 stu2-3HA-IAA7:KanMX DSN1-HIS-FLAG:URA3*
M2248	*MAT**a** leu2::pSTU2-stu2(S813A S815A)-GFP:LEU2 his3::pGPD1-OsTIR1:HIS3 stu2-3HA-IAA7:KanMX DSN1-HIS-FLAG:URA3*
M2249	*MAT**a** leu2::pSTU2-stu2(S813D S815D)-GFP:LEU2 his3::pGPD1-OsTIR1:HIS3 stu2-3HA-IAA7:KanMX DSN1-HIS-FLAG:URA3*
M2250	*MAT**a** leu2::pSTU2-stu2(K598A R599A S813A S815A)-GFP:LEU2 his3::pGPD1-OsTIR1:HIS3 stu2-3HA-IAA7:KanMX DSN1-HIS-FLAG:URA3*
M2251	*MAT**a** leu2::pSTU2-stu2(K598A R599A S813D S815D)-GFP:LEU2 his3::pGPD1-OsTIR1:HIS3 stu2-3HA-IAA7:KanMX DSN1-HIS-FLAG:URA3*
M2298	*MAT**a** leu2::pSTU2-STU2-GFP:LEU2 stu2-3V5-IAA7:KanMX trp1::pGPD1-OsTIR1:TRP1 NUP2-mKATE2:HisMX6*
M2301	*MAT**a** leu2::pSTU2-stu2(Δ560-657::GDGAGL^{linker}-(592-606)-GDGAGL^{linker})-GFP:LEU2 his3::pGPD1-OsTIR1:HIS3 stu2-3HA-IAA7:KanMX DSN1-HIS-FLAG:URA3*
M2302	*MAT**a** leu2::pSTU2-stu2(Δ560-657::GDGAGL^{linker}-(592-606)-GDGAGL^{linker})-PKKKRKV$^{SV40\ NLS}$-GFP:LEU2 his3::pGPD1-OsTIR1:HIS3 stu2-3HA-IAA7:KanMX DSN1-HIS-FLAG:URA3*
M2350	*MAT**a** stu2-3V5-IAA7:KanMX trp1::pGPD1-OsTIR1:TRP1 KAP60-3FLAG:His3MX*
M2351	*MAT**a** leu2::pSTU2-stu2(S603A)-GFP:LEU2 stu2-3V5-IAA7:KanMX trp1::pGPD1-OsTIR1:TRP1 NUP2-mKATE2:HisMX6*
M2353	*MAT**a** leu2::pSTU2-stu2(K598A R599A)-PKKKRKV$^{SV40\ NLS}$-GFP:LEU2 stu2-3V5-IAA7:KanMX cdc20-AID:KanMX trp1::pGPD1-OsTIR1:TRP1 NUP2-mKATE2:HisMX6*
M2390	*MAT**a** leu2::pSTU2-GFP-GST:LEU2 stu2-3V5-IAA7:KanMX cdc20-AID:KanMX trp1::pGPD1-OsTIR1:TRP1 NUP2-mKATE2:HisMX6*
M2391	*MAT**a** leu2::pSTU2-PKKKRKV$^{SV40\ NLS}$-GFP-GST:LEU2 stu2-3V5-IAA7:KanMX cdc20-AID:KanMX trp1::pGPD1-OsTIR1:TRP1 NUP2-mKATE2:HisMX6*
M2392	*MAT**a** leu2::pSTU2-stu2(592-607)-GFP-GST:LEU2 stu2-3V5-IAA7:KanMX cdc20-AID:KanMX trp1::pGPD1-OsTIR1:TRP1 NUP2-mKATE2:HisMX6*
M2435	*MAT**a** leu2::pSTU2-STU2-3V5:LEU2 stu2-3V5-IAA7:KanMX trp1::pGPD1-OsTIR1:TRP1 KAP60-3FLAG:His3MX*
M2436	*MAT**a** leu2::pSTU2-stu2(K598A R599A)-3V5:LEU2 stu2-3V5-IAA7:KanMX trp1::pGPD1-OsTIR1:TRP1 KAP60-3FLAG:His3MX*
M2437	*MAT**a** leu2::pSTU2-stu2(592-607(K598 R599))-GFP-GST:LEU2 stu2-3V5-IAA7:KanMX CDC20-AID:KanMX trp1::pGPD1-OsTIR1:TRP1 NUP2-mKATE2:HisMX6*
M2438	*MAT**a** leu2::pSTU2-stu2(592-607(S603A))-GFP-GST:LEU2 stu2-3V5-IAA7:KanMX cdc20-AID:KanMX trp1::pGPD1-OsTIR1:TRP1 NUP2-mKATE2:HisMX6*

M2443	*MAT**a** leu2::pSTU2-stu2(592-607)-GFP-GST:LEU2 stu2-3V5-IAA7:KanMX trp1::pGPD1-OsTIR1:TRP1 NUP2-mKATE2:HisMX6*
M2480	*MAT**a** leu2::pSTU2-stu2(592-607)-GFP(A206K)-GST:LEU2 stu2-3V5-IAA7:KanMX cdc20-AID:KanMX trp1::pGPD1-OsTIR1:TRP1 NUP2-mKATE2:HisMX6*
M2726	*MAT**a** leu2::pSTU2-stu2(592-607(S603E))-GFP-GST:LEU2 stu2-3V5-IAA7:KanMX cdc20-AID:KanMX trp1::pGPD1-OsTIR1:TRP1 NUP2-mKATE2:HisMX6*
M2729	*MAT**a** leu2::pSTU2-STU2-PKKKRKV$^{SV40\ NLS}$-GFP:LEU2 trp1::pGPD1-OsTIR1:TRP1 SPC110-mCherry:HygMX stu2-3V5-IAA7:KanMX*
M2731	*MAT**a** leu2::pSTU2-stu2(Δ560-657)-PKKKRKV$^{SV40\ NLS}$-GFP:LEU2 trp1::pGPD1-OsTIR1:TRP1 SPC110-mCherry:HygMX stu2-3V5-IAA7:KanMX*
M2846	*MAT**a** leu2::pSTU2-stu2(Δ592-606)-GFP:LEU2 his3::pGPD1-OsTIR1:HIS3 stu2-3HA-IAA7:KanMX DSN1-HIS-FLAG:URA3*

Supplementary Table 1B. Strains used in this study that are derivatives of M1652 (S288C)

M1652	*MAT**a** ura3-52 leu2-3,112 his3^{200} lys2-801 am*
M2166	*MAT**a** his3::pGPD1-OsTIR1:HIS3 stu2-3HA-IAA7:KanMX GFP-TUB1:URA3 cdc23-1*
M2231	*MAT**a** leu2::pSTU2-STU2-Halo-3V5:LEU2 his3::pGPD1-OsTIR1:HIS3 stu2-3HA-IAA7:KanMX GFP-TUB1:URA3 cdc23-1*
M2232	*MAT**a** leu2::pSTU2-stu2(K598A R599A)-Halo-3V5:LEU2 his3::pGPD1-OsTIR1:HIS3 stu2-3HA-IAA7:KanMX GFP-TUB1:URA3 cdc23-1*
M2234	*MAT**a** leu2::pSTU2-stu2(Δ592-606)-Halo-3V5:LEU2 his3::pGPD1-OsTIR1:HIS3 stu2-3HA-IAA7:KanMX GFP-TUB1:URA3 cdc23-1*
M2360	*MAT**a** leu2::pSTU2-stu2(Δ560-657:GDGAGL^{linker})-Halo-3V5:LEU2 his3::pGPD1-OsTIR1:HIS3 stu2-3HA-IAA7:KanMX GFP-TUB1:URA3 cdc23-1*
M3516	*MAT**a** leu2::pSTU2-stu2(Δ560-657:GDGAGL^{linker})-PKKKRKV$^{SV40\ NLS}$-Halo-3V5: LEU2 his3::pGPD1-OsTIR1:HIS3 stu2-3HA-IAA7:KanMX GFP-TUB1:URA3 cdc23-1*

Supplementary Table 2. Plasmids and Primers used in this study.

STU2-3V5 variants were constructed by mutagenizing pM225 as described in (Liu & Naismith, 2008; Tseng et al., 2008), resulting in pM235 (*pSTU2-stu2(Δ560–657*::*GDGAGL*^{linker}*)-3V5*, i.e. *stu2*$^{\Delta BL}$), pM310 (*pSTU2-stu2(S603A)-3V5*, i.e. *stu2*^{S603A}), pM338 (*pSTU2-stu2(Δ592-606)-3V5*, i.e. *stu2*$^{\Delta 592\text{-}606}$), pM465 (*pSTU2-stu2(K598A)-3V5*, i.e. *stu2*^{K598A}), pM466 (*pSTU2-stu2(R599A)-3V5*, i.e. *stu2*^{R599A}), pM491 (*pSTU2-stu2(K598A R599A)-3V5*, i.e. *stu2*$^{KR/AA}$), pM513 (*pSTU2-stu2(P596A)-3V5*, i.e. *stu2*^{P596A}), pM514 (*pSTU2-stu2(S597A)-3V5*, i.e. *stu2*^{S597A}), pM522 (*pSTU2-stu2(V600A S602A)-3V5*, i.e. *stu2*$^{V600A\ S602A)}$, pM536 (*pSTU2-stu2(ΔBL::GDGAGL*^{linker}*-(592-606(P604A L605A R606A))-GDGAGL*^{linker}*)-3V5*), pM537 (*pSTU2-stu2(ΔBL::GDGAGL*^{linker}*-(592-606(S592A S593A V594A L595A))-GDGAGL*^{linker}*)-3V5*), and pM630 (*pSTU2-STU2-Halo-3V5*). *STU2-Halo-3V5* variants were constructed by mutagenizing pM630 as described in (Liu & Naismith, 2008; Tseng et al., 2008), resulting in pM655 (*pSTU2-stu2(K598A R599A)-Halo-3V5*, i.e. *stu2*$^{KR/AA}$), pM656 (*pSTU2-stu2(Δ592-606)-Halo-3V5*, i.e. *stu2*$^{\Delta 592\text{-}606}$), pM657 (*pSTU2-stu2(ΔBL::GDGAGL*^{linker}*-(592-606)-GDGAGL*^{linker}*)-Halo-3V5*, i.e. *stu2*$^{\Delta BL::592\text{-}606}$), pM776 (*pSTU2-stu2(Δ560–657*::*GDGAGL*^{linker}*)-Halo-3V5*, i.e. *stu2*$^{\Delta BL}$). *pSTU2-STU2-GFP* is described in (Miller et al., 2019). *STU2-GFP* variants were constructed by mutagenizing pM488 as described in (Liu & Naismith, 2008; Tseng et al., 2008) resulting in pM585 (*pSTU2-stu2(Δ560–657*::*GDGAGL*^{linker}*)-GFP*, i.e. *stu2*$^{\Delta BL}$), pM586 (*pSTU2-stu2(Δ592-606)-GFP*, i.e. *stu2*$^{\Delta 592\text{-}606}$), pM647 (*pSTU2-stu2(S813A S815A)-GFP*, i.e. *stu2*$^{S813A\ S815A}$), pM648 (*pSTU2-stu2(S813D S815D)-GFP*, i.e. *stu2*$^{S813D\ S815D}$), pM649 (*pSTU2-stu2(K598A R599A S813A S815A)-GFP*, i.e. *stu2*$^{KR/AA\ S813A\ S815A}$), pM650 (*pSTU2-stu2(K598A R599A S813D S815D)-GFP*, i.e. *stu2*$^{KR/AA\ S813D\ S815D}$), pM659 (*pSTU2-STU2-PKKKRKV*^{SV40_NLS}*-GFP*, i.e. *STU2*^{WT}*-NLS*^{SV40}), pM661 (*pSTU2-stu2(ΔBL:GDGAGL*^{linker}*)-PKKKRKV*^{SV40_NLS}*-GFP*, i.e. *stu2*$^{\Delta BL}$*-NLS*^{SV40}), pM703 (*pSTU2-stu2(S603A)-GFP*, i.e. *stu2*^{S603A}), pM709 (*pSTU2-stu2(K598A R599A)-PKKKRKV*^{SV40_NLS}*-GFP*, i.e. *stu2*$^{KR/AA}$*-NLS*^{SV40}), pM742 (*pSTU2-stu2(ΔBL::GDGAGL*^{linker}*-(592-606)-GDGAGL*^{linker}*)-GFP*, i.e. *stu2*$^{\Delta BL::592\text{-}606}$), pM743 (*pSTU2-stu2(ΔBL::GDGAGL*^{linker}*-(592-606)-GDGAGL*^{linker}*)-PKKKRKV*^{SV40_NLS}*-GFP*, i.e. *stu2*$^{\Delta BL::592\text{-}606}$*-NLS*^{SV40}), pM1406 (*pSTU2-stu2(Δ592-606)-GFP*, i.e. *stu2*$^{\Delta 592\text{-}606}$), pM772 (*pSTU2-GFP-GST*), pM773 (*pSTU2-NLS*^{SV40}*-GFP-GST*), and pM774 (*pSTU2-stu2*$^{592\text{-}607}$*-GFP-GST*). *stu2*$^{592\text{-}607}$*-GFP-GST* variants were constructed by mutagenizing pM774 as described in (Liu & Naismith, 2008; Tseng et al., 2008), resulting in pM1361 (pSTU2-*stu2(592-607(K598A R599A))-GFP-GST*, i.e. *stu2*$^{592\text{-}607(KR/AA)}$), pM1362 (pSTU2-*stu2(592-607(S603A))-GFP-GST*, i.e. *stu2*$^{592\text{-}607(S603A)}$), and pM1410 (pSTU2-*stu2(592-607(S603E))-GFP-GST*, i.e. *stu2*$^{592\text{-}607(S603E)}$).

Plasmid	Primers used to generate plasmids (5' to 3'):	
pM225 (pSTU2-STU2-3V5, i.e. *STU2*^{WT})	SB4372	GATCGATCgggcccTAGTACAATTTCTAATGGGC
	SB4374	GATCGATCctcgagTTATGGATCTGTACTATCCAGTCC
pM235 (pSTU2-stu2(Δ560-657::GDGAGL^{linker})-3V5, i.e. *stu2*$^{\Delta BL}$*)*	SB4411	GGAAAAAAATTGAAGAAACGGTCAAAACTggtgatggtgctggtttgGAAAAGTTGATTGAAGAATACAAGTACAGAC
	SB4413	ggatccactagttctagagc
pM310 (pSTU2-stu2(S603A)-3V5, i.e. *stu2*^{S603A}*)*	SB5093	GTACTTCCCTCCAAGAGAGTGGCATCTgCACCGCTGAGAAATGATAACAAAAGTAAAGTG
	SB4371	GTTGACGTCCTCTTTCCTTC
pM338 (pSTU2-stu2(Δ592-606)-3V5, i.e. *stu2*$^{\Delta 592-606}$*)*	SB5247	CTGGGCCAATGGAGAATAAATTTCTCCTGAAAAAAaatgataacaaaagtaaagtgaacc
	SB4413	ggatccactagttctagagc
pM339 (pSTU2-stu2(Δ633-648)-3V5, i.e. *stu2*$^{\Delta 633-648}$)	SB4413	ggatccactagttctagagc
	SB5249	CCGCATCAAAACCATCAATGGTAGCTGCTAACAATaacgtagtagctaatagcactgac
pM455 (pSTU2-stu2(K598A R599A)-3V5, i.e. *stu2*$^{KR/AA}$*)*	SB4413	ggatccactagttctagagc
	SB5349	CCTGAAAAAAAGTTCTGTACTTCCCTCCgcggcaGTGGCATCTTCACCGCTGAGAAATG
pM465 (pSTU2-stu2(K598A)-3V5, i.e. *stu2*^{K598A}*)*	SB5458	CCTGAAAAAAAGTTCTGTACTTCCCTCCgcgAGAGTGGCATCTTCACCGCTGAGAAATG
	SB4413	ggatccactagttctagagc
pM466 (pSTU2-stu2(R599A)-3V5, i.e. *stu2*^{R599A}*)*	SB5459	CCTGAAAAAAAGTTCTGTACTTCCCTCCAAGgcaGTGGCATCTTCACCGCTGAGAAATG
	SB4413	ggatccactagttctagagc
pM481 (pSTU2-stu2(Δ560-657::GDGAGL^{linker}-(592-606)-GDGAGL^{linker})-3V5, i.e. *stu2*$^{\Delta BL::592-606}$)	SB5519	cattagagcacttggataatttgaaaaggAAAAAAATTGAAGAAACGGTCAAAACTggtgatggtgctggtttgagttctgtacttc
	SB5520	gaagtacagaactcaaaccagcaccatcaccAGTTTTGACCGTTTCTTCAATTTTTTTcctttcaaattatccaagtgctctaatg
pM488 (pSTU2-STU2-GFP, i.e. *STU2*^{WT})	SB3988	GAAAAAATGAAGGCCAAATCAAGGCGGGAAGGGACAACCAGGACGcggatccccgggttaattaa

	SB5918	cgataccgtcgaccacctgccttgctccctcgag TTATTTGTATAGTTCATCCATGCC
pM491 (pSTU2-stu2(K598A R599A)-GFP, i.e. *stu2$^{KR/AA}$)*	SB3988	GAAAAAATGAAGGCCAAATCAAG GCGGGAAGGGACAACCAGGACG cggatccccgggttaattaa
	SB5918	cgataccgtcgaccacctgccttgctccctcgag TTATTTGTATAGTTCATCCATGCC
pM513 (pSTU2-stu2(P596A)-3V5, i.e. *stu2^{P596A})*	oMM17	ggatccactagttctagagc
	oMM21	GGAGAATAAATTTCTCCTGAAAAA AAGTTCTGTACTTgccTCCAAGAG AGTGGCATCTTC
pM514 (pSTU2-stu2(S597A)-3V5, i.e. *stu2^{S597A})*	oMM17	ggatccactagttctagagc
	oMM22	GAATAAATTTCTCCTGAAAAAAAG TTCTGTACTTCCCgcaAAGAGAGT GGCATCTTCACC
pM518 (pSTU2-stu2(Δ560-657::GDGAGL^{linker}-(596-599)-GDGAGL^{linker})-3V5, i.e. *stu2$^{\Delta BL::596-599}$)*	oMM17	ggatccactagttctagagc
	oMM27	CTGGTGATGGTGCTGGTTTGccctc caagagaGGAGACGGAGCAGGCTT AGAAAAG
pM522 (pSTU2-stu2(V600A S602A)-3V5, i.e. *stu2$^{V600A\ S602A}$)*	oMM17	ggatccactagttctagagc
	oMM73	CTGTACTTCCCTCCAAGAGAgcag cagcTTCACCGCTGAGAAATGATA AC
pM536 (pSTU2-stu2(Δ560-657::GDGAGL^{linker}-(592-606(P604A L605A R606A))-GDGAGL^{linker})-3V5, i.e. *stu2$^{P604A\ L605A\ R606}$*)	oMM17	ggatccactagttctagagc
	oMM131	CTTCCCTCCAAGAGAGTGGCATC TTCAgcagcagcaGGAGACGGAGCA GGCTTAGAAAAG
pM537 (pSTU2-stu2(Δ560-657::GDGAGL^{linker}-(592-606(S592A S593A V594A L595A))-GDGAGL^{linker})-3V5, i.e. *stu2$^{S592A\ S593A\ V594A\ L595A}$*)	oMM17	ggatccactagttctagagc
	oMM132	GGTCAAAACTGGTGATGGTGCTG GTTTGgcagcagcagcaCCCTCCAAG AGAGTGGCATC

pM585 (pSTU2-stu2(Δ560-657)-GFP, i.e. *stu2$^{\Delta BL}$)*	oMM10	gatgagggggaatatcagatag
	oMM16	GTTGACGTCCTCTTTCCTTC
pM589 (pSTU2-stu2(Δ560-657::GDGAGL^{linker}-(596-604)-GDGAGL^{linker})-3V5, i.e. *stu2$^{\Delta BL::596-604}$)*	oMM16	GTTGACGTCCTCTTTCCTTC
	oMM195	CTggtgatggtgctggtttgCCCTCCAAGAGAGTGGCATCTTCACCGggagacggagcaggcttaGAAAAG
pM630 (pSTU2-STU2-Halo-3V5, i.e. *STU2^{WT}*)	oMM20	AATGAAGGCCAAATCAAGGCGGGAAGGGACAACCAGGACGcggatcccccgggttaattaa
	oMM205	CCtggatccactagttctagagcggccgcGCCGGAAATCTCGAGCGTCGACAGCCAGCGC
pM647 (pSTU2-stu2(S813A S815A)-GFP, i.e. *stu2$^{S813A\ S815A}$)*	oMM10	gatgagggggaatatcagatag
	oMM160	CGCGGTGCGGCAGGTCGCCGATagcCTCggcTGATCTTCTTTCATAGTTGACGTCC
pM648 (pSTU2-stu2(S813D S815D)-GFP, i.e. *stu2$^{S813D\ S815D}$)*	oMM10	gatgagggggaatatcagatag
	oMM161	CGCGGTGCGGCAGGTCGCCGATatcCTCatcTGATCTTCTTTCATAGTTGACGTCC
pM649 (pSTU2-stu2(K598A R599A S813A S815A)-GFP, i.e. *stu2$^{KR/AA\ S813A\ S815A}$)*	oMM10	gatgagggggaatatcagatag
	oMM161	CGCGGTGCGGCAGGTCGCCGATatcCTCatcTGATCTTCTTTCATAGTTGACGTCC
pM650 (pSTU2-stu2(K598A R599A S813D S815D)-GFP, i.e. *stu2$^{KR/AA\ S813D\ S815D}$)*	oMM10	gatgagggggaatatcagatag
	oMM161	CGCGGTGCGGCAGGTCGCCGATatcCTCatcTGATCTTCTTTCATAGTTGACGTCC
pM655 (pSTU2-stu2(K598A R599A)-Halo-3V5, i.e. *stu2$^{KR/AA}$)*	oMM10	gatgagggggaatatcagatag
	oMM16	GTTGACGTCCTCTTTCCTTC
pM656 (pSTU2-stu2(Δ592-606)-Halo-3V5, i.e. *stu2$^{\Delta 592-606}$)*	oMM10	gatgagggggaatatcagatag

	oMM16	GTTGACGTCCTCTTTCCTTC
pM659 (pSTU2-STU2-PKKKRKV$^{SV40\ NLS}$-GFP, i.e. *STU2^{WT}-NLS^{SV40})*	oMM2	tatcgcactcacgtaaacac
	oMM252	GGGAAGGGACAACCAGGACGggtgatggtgctggtttgccaaagaagaaaagaaaggtaggagacggagcaggcttaagtaaaggagaagaacttttc
pM661 (pSTU2-stu2(Δ560-657:GDGAGL^{linker})-PKKKRKV$^{SV40\ NLS}$-GFP, i.e. *stu2^{ΔBL}-NLS^{SV40})*	oMM2	tatcgcactcacgtaaacac
	oMM252	GGGAAGGGACAACCAGGACGggtgatggtgctggtttgccaaagaagaaaagaaaggtaggagacggagcaggcttaagtaaaggagaagaacttttc
pM703 (pSTU2-stu2(S603A)-GFP, i.e. *stu2^{S603A})*	oMM10	gatgagggggaatatcagatag
	oMM16	GTTGACGTCCTCTTTCCTTC
pM709 (pSTU2-stu2(K598A R599A)-PKKKRKV$^{SV40\ NLS}$-GFP, i.e. *stu2$^{KR/AA}$-NLS^{SV40})*	oMM10	gatgagggggaatatcagatag
	oMM16	GTTGACGTCCTCTTTCCTTC
pM742 (pSTU2-stu2(Δ560-657::GDGAGL^{linker}-(592-606)-GDGAGL^{linker})-GFP, i.e. *stu2$^{ΔBL::592-606}$)*	oMM10	gatgagggggaatatcagatag
	oMM16	GTTGACGTCCTCTTTCCTTC
pM743 (pSTU2-stu2(Δ560-657::GDGAGL^{linker}-(592-606)-GDGAGL^{linker})-PKKKRKV$^{SV40\ NLS}$-GFP, i.e. *stu2$^{ΔBL::592-606}$-NLS^{SV40})*	oMM10	gatgagggggaatatcagatag
	oMM16	GTTGACGTCCTCTTTCCTTC
pM772 (pSTU2-GFP-GST, i.e. *GFP-GST*)	oMM341	ggcatggatgaactatacaaaGGCGGGAGCGGCGGGGGAAGTGGAtcccctatactaggttattgg
	oMM342	ccacctgccttgctccctcgagTTAacgcggaaccagatccg
pM773 (pSTU2-PKKKRKV$^{SV40\ NLS}$-GFP-GST, i.e. *NLS^{SV40}-GFP-GST*)	oMM341	ggcatggatgaactatacaaaGGCGGGAGCGGCGGGGGAAGTGGAtcccctatactaggttattgg

	oMM342	ccacctgccttgctccctcgagTTAacgcggaaccagatccg
pM774 (pSTU2-stu2(592-607)-GFP-GST, i.e. *stu2$^{592-607}$-GFP-GST)*	oMM341	ggcatggatgaactatacaaaGGCGGGAGCGGCGGGGGAAGTGGAtcccctatactaggttattgg
	oMM342	ccacctgccttgctccctcgagTTAacgcggaaccagatccg
pM776 (pSTU2-stu2(Δ560-657:GDGAGL^{linker})-Halo-3V5, i.e. *stu2^{ΔBL})*	oMM10	gatgagggggaatatcagatag
	oMM16	GTTGACGTCCTCTTTCCTTC
pM1361 (pSTU2-stu2(592-607(K598A R599A))-GFP-GST, i.e. *stu2$^{592-607(KR/AA)}$)*	oMM8	CCTAGCAACCTTTCGCGCAAG
	oMM390	ctcagcggtgaagatgccacTGCCGCggagggaagtacagaactcatag
pM1362 (pSTU2-stu2(592-607(S603A))-GFP-GST, i.e. *stu2$^{592-607(S603A)}$*)	oMM8	CCTAGCAACCTTTCGCGCAAG
	oMM391	CGGGGATCCGatttctcagcggtgcagatgccactctcttggagggaag
pM1363 (pStu2-stu2(592-607)-GFP(A206K)-GST, i.e. *stu2$^{592-607}$-GFP(A206K)-GST)*	oMM401	cttttaccagacaaccattacctgtccacacaatctAAActttcgaaagatcccaacgaaaag
	oMM405	ccatgtataaaacaacatcaag
pM1406 (pSTU2-stu2(Δ592-606)-GFP, i.e. *stu2$^{Δ592-606}$)*	oMM2	tatcgcactcacgtaaacac
	oMM11	AGTGAACCCAATAGGGTCAG
pM1410 (pSTU2-stu2(592-607(S603E))-GFP-GST, i.e. *stu2$^{592-607(S603E)}$*)	oMM8	CCTAGCAACCTTTCGCGCAAG
	oMM392	CGGGGATCCGatttctcagcggctcagatgccactctcttggagggaag
pM1486 (pSTU2-stu2(Δ560-657:GDGAGL^{linker})-PKKKRKV$^{SV40\ NLS}$-Halo-3V5, i.e. *stu2^{ΔBL}-NLS^{SV40}*	oMM2	tatcgcactcacgtaaacac
	oMM365	gccaaagaagaaaagaaaggtaggagacggagcaggcttaGCAGAAATCGGTACTGGCTTTC